

Simulation of the 1d XY model on a quantum computer

Marc Farreras^{1,2*}, Alba Cervera-Lierta^{2†}

¹Leiden Institute of Advanced Computer Science (LIACS), Leiden University, Leiden 2333 CA, The Netherlands

²Barcelona Supercomputing Center, Plaça Eusebi Güell, 1-3, 08034 Barcelona, Spain

* m.farreras.i.bartra@liacs.leidenuniv.nl, † alba.cervera@bsc.es

Abstract

The field of quantum computing has grown fast in recent years, both in theoretical advancements and the practical construction of quantum computers. These computers were initially proposed, among other reasons, to efficiently simulate and comprehend the complexities of quantum physics. **In this paper, we present a comprehensive scheme for the exact simulation of the 1-D XY model on a quantum computer.** We successfully diagonalize the proposed Hamiltonian, enabling access to the complete energy spectrum. Furthermore, we propose a novel approach to design a quantum circuit to perform exact time evolution. Among all the possibilities this opens, we compute the ground and excited state energies for the symmetric XY model with spin chains of $n = 4$ and $n = 8$ spins. Further, we calculate the expected value of transverse magnetization for the ground state in the transverse Ising model. Both studies allow the observation of a quantum phase transition from an antiferromagnetic to a paramagnetic state. Additionally, we have simulated the time evolution of the state all spins up in the transverse Ising model. The scalability and high performance of our algorithm make it an ideal candidate for benchmarking purposes, while also laying the foundation for simulating other integrable models on quantum computers.

Copyright attribution to authors.

This work is a submission to SciPost Physics.

License information to appear upon publication.

Publication information to appear upon publication.

12/12/2024

Accepted Date

Published Date

1

2 Contents

3	1 Introduction	2
4	2 The 1 – D XY model	3
5	2.1 Jordan-Wigner transformation	4
6	2.2 Fermionic Fourier Transform (fFT)	8
7	2.3 Bogoliubov Transformation	10
8	3 Quantum circuit to diagonalize the XY model	12

9	3.1 Jordan-Wigner circuit	13
10	3.2 Fermionic Fourier transform circuit	14
11	3.3 Bogoulibov transformation gate	20
12	3.4 Example: $n = 4$ and $n = 8$ spin chain	24
13	4 Time evolution	25
14	5 Results and discussion	29
15	6 Conclusion	30
16	References	32
17		
18		

19 **1 Introduction**

20 In the first decade of the XXI century, we witnessed an explosion of the quantum computing field
21 driven by the incredible potential that quantum computing exhibits to solve some intractable clas-
22 sical problems [1]. Among these challenges, one of the enduring objectives of quantum computing
23 is the simulation of quantum systems. Although several classical strategies exist for simulating such
24 systems [2,3], they often prove to be inefficient when dealing with complex quantum systems. Con-
25 sequently, the simulation of quantum systems demands alternative methods for efficient execution.
26 Here, quantum computers emerge as a promising solution, since due to their quantum nature the
27 simulation of strongly correlated systems is the natural arena where quantum computers are ex-
28 pected to show a clear advantage over classical ones, as Feynman stated in Ref. [4].

29 Despite having undergone considerable development during the last decade, quantum computing
30 is still in an early stage. The current state of quantum computing is known as the Noisy Intermediate-
31 Scale Quantum (NISQ) era [5]. The NISQ era has been characterized by constrained-size quantum
32 processors (containing 100 qubits approximately) with imperfect control over them; they are sensi-
33 tive to their environment and prone to quantum decoherence and other sources of errors. **Despite**
34 **these challenges, researchers have successfully pushed the boundaries of current quantum technol-**
35 **ogy, particularly in the simulation of physical systems [6]. This progress has been largely enabled**
36 **by the development of error mitigation techniques and the optimization of quantum circuits [7, 8],**
37 **where more hardware-faithful implementations have been prioritized over error-prone alternatives.**
38 **Nevertheless, these methods require thorough characterization of the underlying quantum hard-**
39 **ware, making it essential to develop scalable and standardized benchmarking techniques. Such**
40 **benchmarks are crucial for both companies and researchers to evaluate and compare the efficiency**
41 **of emerging quantum devices.**

42 This paper presents a circuit **suitable for the NISQ era**, offering the capability to explore intriguing
43 phenomena such as quantum phase transitions. Our work consists of implementing a quantum circuit
44 that performs the exact simulation of a 1-D spin chain with an XY -type interaction. We programmed
45 a set of Python libraries that allows the implementation of the circuit for systems with a power of
46 2 number of qubits using Qibo [9], an open-source framework for quantum computing. Moreover,

47 Qibo is the native language of the Barcelona Supercomputing Center quantum computer, which will
 48 allow the users to directly test this algorithm with real machines. The foundation of our work is
 49 based on Ref. [10, 11], where the steps followed to design the quantum circuit rest upon tracing and
 50 implementing the well-known transformations that solve the model analytically [12]. As a result, this
 51 technique can access the whole spectrum, enabling us to simulate any excited or thermal state and its
 52 dynamical evolution. In addition, this framework can be easily extended to other integrable models,
 53 including the Kitaev-honeycomb model [13], or to systems whose effective low-energy behavior can
 54 be suitably described by quasi-particles [14].

55 This paper is organized as follows: In Sec.2 we describe the characteristics of the XY model and
 56 solve it analytically. Moving to Sec.3, we revisit the method introduced in Ref. [10] to construct
 57 an efficient circuit that diagonalizes the XY Hamiltonian. We then present the circuit employed for
 58 simulating spin chains of $n = 4$ and $n = 8$ qubits. Next, in Sec.4 we design a quantum circuit tailored
 59 for exact time evolution. Our simulations, utilizing the proposed quantum circuit, are detailed in
 60 Sec.5. Finally, the conclusions are exposed in Sec.6 and the code is available in Ref. [15].

61 2 The 1 – D XY model

62 The XY model is derived from the Heisenberg model [16] by introducing an easy-plane anisotropy.
 63 Those models are widely used to study critical points and phase transitions of magnetic systems
 64 within the condensed matter field. The 1 – D XY Hamiltonian can be written as

$$\mathcal{H}_{XY} = J \left(\sum_{i=1}^n \frac{1+\gamma}{2} \sigma_i^x \sigma_{i+1}^x + \frac{1-\gamma}{2} \sigma_i^y \sigma_{i+1}^y \right) + \lambda \sum_{i=1}^n \sigma_i^z \quad (1)$$

65 where n is the number of spins in the 1-D spin chain, σ_j^i with $i = x, y, z$ are the Pauli matrix acting
 66 on the site j , J determine the behavior of the ordered phase, ferromagnetic for $J < 0$ and antifer-
 67 romagnetic $J > 0$, γ is the anisotropic parameter and λ represents the strength of the transverse
 68 magnetic field.

69 One important feature for which the XY model stands out is that it exhibits a quantum phase
 70 transition [17, 18]. **These transitions occur at zero temperature** and stem from the competition of
 71 the different terms within the Hamiltonian, regulated by a non-thermal physical parameter of the
 72 system. At zero temperature, each term presents a specific ground state, and the properties of these
 73 ground states dictate the phase of the system.

74 Specifically for the 1 – D XY model, the Hamiltonian presents three terms with ground states that
 75 exhibit different phases. The first two terms parametrized by J and γ are $\sigma_i^x \sigma_{i+1}^x$ and $\sigma_i^y \sigma_{i+1}^y$. Both
 76 by themselves correspond to the well-known Ising model, in which the ground state is ferromagnetic
 77 or antiferromagnetic, depending on the sign of J , and points respectively to the x or y axis. Con-
 78 trarily, the ground state of the third term σ_i^z , parametrized by λ is paramagnetic and points to the
 79 z axis. As a result, the ground state will show ferromagnetic or antiferromagnetic behavior when
 80 $|J| > \lambda$ and the direction of the spin will be mediated by γ . However, the ground state will show
 81 paramagnetic behavior for $|J| < \lambda$. In Fig.1 there is shown the phase diagram at $T = 0$ of the 1-D
 82 XY model for $J = -1$.

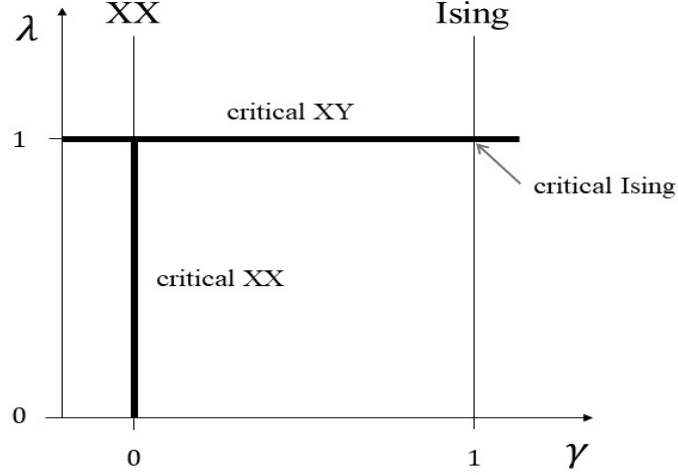


Figure 1: Phase diagram of the quantum XY model.

83 In the next subsections, we derive the analytical solution of the XY model. However, before start-
 84 ing is convenient to rewrite Eq. (1) it in terms of **spin ladder** operators $\sigma^{+(-)}$ which increase(decrease)
 85 the projection of the third component of the spin S_z by 1. The σ^x and σ^y operators then can be writ-
 86 ten as

$$\begin{aligned}
 \sigma^x &= \sigma^+ + \sigma^-, \\
 \sigma^y &= -i(\sigma^+ - \sigma^-), \\
 \sigma^z &= 2\sigma^+ \sigma^- - 1.
 \end{aligned} \tag{2}$$

87 Hence, the Hamiltonian from Eq.(1) becomes

$$\mathcal{H}'_{XY} = J \left(\sum_{i=1}^{n-1} \sigma_i^+ \sigma_{i+1}^- + \sigma_i^- \sigma_{i+1}^+ + \gamma (\sigma_i^+ \sigma_{i+1}^+ + \sigma_i^- \sigma_{i+1}^-) \right) + \lambda \sum_{i=1}^n (2\sigma_i^+ \sigma_i^- - 1). \tag{3}$$

88
 89 Furthermore, it is worth remembering some properties from the Spin $\frac{1}{2}$, which will be used later
 90 on in the next steps.

$$\begin{aligned}
 \sigma^+ (-\sigma^z) &= \sigma^+, & \sigma^- (-\sigma^z) &= -\sigma^-, \\
 -\sigma^z \sigma^+ &= -\sigma^+, & -\sigma^z \sigma^- &= \sigma^-.
 \end{aligned} \tag{4}$$

91 2.1 Jordan-Wigner transformation

92 Generally, quantum spin objects are notoriously difficult to deal with in many-body physics because
 93 they neither fulfill fermionic nor bosonic algebra. For this reason, the first step to diagonalize XY
 94 Hamiltonian consists of applying the Jordan-Wigner transformation [19] which maps the spin oper-
 95 ators σ into spinless fermionic modes c .

96 The Jordan-Wigner transformation takes advantage of the similarities between fermions and spin
 97 operators. The existence of the stated similarity can be noticed by how both operators act on their
 98 respective basis, where fermionic basis $|1\rangle$ and $|0\rangle$ respectively corresponds to having one or no
 99 fermion in the state (no fermion state is also called void), while $|+\rangle$ and $|-\rangle$ means having a spin
 100 pointing up or down in the z axis. As shown in Table 1, there is a clear equivalence between $|0\rangle$ and
 101 $|-\rangle$, and the same with $|1\rangle$ and $|+\rangle$.

Fermions	Spin $\frac{1}{2}$
$c^\dagger 0\rangle = 1\rangle$	$\sigma^+ -\rangle = +\rangle$
$c^\dagger 1\rangle = 0$	$\sigma^+ +\rangle = 0$
$c 0\rangle = 0$	$\sigma^- -\rangle = 0$
$c 1\rangle = 0\rangle$	$\sigma^- +\rangle = -\rangle$

Table 1: Fermionic and Spin operator's behavior when acting in their respective basis.

102 However, there is also an important difference between them, their commutation relationships.
 103 The commutation relationship followed by $\sigma^{+(-)}$ and σ^- operators are

$$\begin{aligned} [\sigma_j^+, \sigma_i^-] &= 0 \quad i \neq j, \\ \{\sigma_i^+, \sigma_j^-\} &= I \quad i = j, \end{aligned} \quad (5)$$

104 while the operators c and c^\dagger obey the fermionic algebra $\{c_i^\dagger, c_j\} = \delta_{ij}$.

105 To solve this problem, Jordan and Wigner introduced an operator, called the string operator
 106 $e^{\pi i \sum_{j=1}^{i-1} \sigma_j^+ \sigma_j^-}$. This operator counts the number of $|+\rangle$ states or fermionic particles in the system and
 107 ensures the addition of a minus sign whenever two fermions are interchanged, thereby enabling the
 108 correct mapping between spin and fermionic operators.

109 Thus, the Jordan-Wigner transformation is defined as

$$\begin{aligned} c_i^\dagger &= \sigma_i^+ e^{-\pi i \sum_{j=1}^{i-1} \sigma_j^+ \sigma_j^-}, \\ c_i &= e^{\pi i \sum_{j=1}^{i-1} \sigma_j^+ \sigma_j^-} \sigma_j^-, \\ c_i^\dagger c_i &= \sigma_j^+ \sigma_j^-. \end{aligned} \quad (6)$$

110 Where the c and c_i^\dagger are the new spinless fermionic operators. Note that $\sigma_j^+ \sigma_j^-$ and $\sigma_i^+ \sigma_i^-$ com-
 111 mute

$$[\sigma_i^+ \sigma_i^-, \sigma_j^-] = -\delta_{ij} \sigma_j^-, \quad [\sigma_i^+ \sigma_i^-, \sigma_j^+] = \delta_{ij} \sigma_j^+, \quad [\sigma_i^+ \sigma_i^-, \sigma_j^+ \sigma_j^-] = 0. \quad (7)$$

112 Therefore,

$$e^{\pm i \pi \sum_{j=n}^m \sigma_j^+ \sigma_j^-} = \prod_{j=n}^m e^{\pm i \pi \sigma_j^+ \sigma_j^-}. \quad (8)$$

113 The next step is to develop the exponential operator

$$e^{\pm i\pi\sigma_j^+\sigma_j^-} = \sum_{l=0}^{\infty} \frac{1}{l!} (\pm i\pi)^l (\sigma_j^+\sigma_j^-)^l = 1 - 2\sigma_j^+\sigma_j^- = -\sigma_j^z. \quad (9)$$

114

115 In consequence, sometimes the Wigner-Jordan transformation is also written as

$$c_i^\dagger = \sigma_i^+ \left(\prod_{l=1}^{i-1} -\sigma_l^z \right), \quad c_i = \left(\prod_{l=1}^{i-1} -\sigma_l^z \right) \sigma_i^-, \quad c_i^\dagger c_i = \sigma_i^+ \sigma_i^-. \quad (10)$$

116

For practical reasons, it is interesting to write down the inverse transformation

$$\sigma_i^+ = c_i^\dagger \left(\prod_{l=1}^{i-1} -\sigma_l^z \right) = c_i^\dagger e^{\pi i \sum_{j=1}^{i-1} \sigma_j^+ \sigma_j^-}, \quad \sigma_i^- = \left(\prod_{l=1}^{i-1} -\sigma_l^z \right) c_i = e^{-\pi i \sum_{j=1}^{i-1} \sigma_j^+ \sigma_j^-} c_i, \quad \sigma_i^z = 2c_i^\dagger c_i - 1. \quad (11)$$

117

Now the transformed spin operators obey the canonical fermion algebra

$$\{c_i, c_j^\dagger\} = \delta_{ij}, \quad \{c_i, c_j\} = 0, \quad \{c_i^\dagger, c_j^\dagger\} = 0, \quad (12)$$

118 as it is shown in Ref. [20].

119

120 Subsequently, let's derive some useful relations. Using Eq.(12) we can to compute the following
121 commutator

$$[c_i^\dagger c_i, c_j^\dagger c_j] = 0 \text{ if } i \neq j. \quad (13)$$

122

For the case $i = j$ the commutator is also 0. Additional useful commutator relations are

$$[c_i^\dagger c_i, c_j] = -\delta_{ji} c_i, \quad [c_i^\dagger c_i, c_j^\dagger] = \delta_{ji} c_i^\dagger, \quad (c_i^\dagger c_i)^2 = c_i^\dagger c_i. \quad (14)$$

123

Applying the different properties derived from the expressions before and $c_i c_i = 0$, one can compute

124

$$\{1 - 2c_i^\dagger c_i, c_i\} = 0, \quad \{1 - 2c_i^\dagger c_i, c_i^\dagger\} = 0. \quad (15)$$

125

Now, using the properties from Eq.(14) and Eq.(15), one can compute the commutation relationship

126

between the string operator described in Eq.(8) and the new fermionic operators

$$\begin{aligned} [e^{\pm i\pi \sum_{j=n}^m c_j^\dagger c_j}, c_i] &= [e^{\pm i\pi \sum_{j=n}^m c_j^\dagger c_j}, c_i^\dagger] = 0, \quad i \notin [n, m], \\ \{e^{\pm i\pi \sum_{j=n}^m c_j^\dagger c_j}, c_i\} &= \{e^{\pm i\pi \sum_{j=n}^m c_j^\dagger c_j}, c_i^\dagger\} = 0, \quad i \in [n, m]. \end{aligned} \quad (16)$$

127

Jordan-Wigner transformation in the XY model

128

Here, we apply the Jordan-Wigner transformation into the elements that appear in the XY Hamiltonian,

129

from Eq.(3). For the $\sigma_i^+ \sigma_{i+1}^+$ term,

$$\sigma_i^+ \sigma_{i+1}^+ = c_i^\dagger c_{i+1}^\dagger, \quad (17)$$

130

where we have taken in count that $c_i^\dagger c_i^\dagger = 0$. Likewise, one can calculate the $\sigma_i^- \sigma_{i+1}^-$ term

$$\sigma_i^- \sigma_{i+1}^- = c_{i+1} c_i. \quad (18)$$

131

Lastly, the $\sigma_i^+ \sigma_{i+1}^-$ and $\sigma_i^- \sigma_{i+1}^+$ can be transformed

$$\sigma_i^+ \sigma_{i+1}^- = c_i^\dagger c_{i+1}, \quad \sigma_i^- \sigma_{i+1}^+ = c_{i+1}^\dagger c_i. \quad (19)$$

132

133 Boundary conditions

134 Until now, we have not mentioned anything about what happens in the boundary terms σ_{n+1} . Given
 135 the finite nature of our simulations, it becomes imperative to establish certain boundary conditions
 136 for our system. Specifically, we've implemented periodic boundary conditions (PBC). However, it's
 137 worth noting that we've opted for a direct application of PBC within the fermionic space. This choice
 138 translates to the relationship between fermionic operators, namely, $c_n c_{n+1} = c_n c_1$.

139 To add this term to our XY Hamiltonian, first, it has to be mapped into the spin space using the
 140 Jordan-Wigner transformation. Unfortunately, this transformation maps the PBC to PBC or antiperi-
 141 odic boundary condition (APBC) depending on whether the system has an odd or even number of
 142 particles or $|+\rangle$ states. Consequently, the boundary term of our Hamiltonian must present this parity
 143 dependence to correctly be mapped into PBC in the fermionic space, this can be achieved using the
 144 $\sigma_1^y \sigma_2^z \cdots \sigma_{n-1}^z \sigma_n^y$ and $\sigma_1^x \sigma_2^z \cdots \sigma_{n-1}^z \sigma_n^x$ terms from Eq.(1). Then the Hamiltonian simulated in this
 145 work reads

$$\mathcal{H}_{XY} = J \left(\sum_{i=1}^{n-1} \frac{1+\gamma}{2} \sigma_i^x \sigma_{i+1}^x + \frac{1-\gamma}{2} \sigma_i^y \sigma_{i+1}^y \right) + \lambda \sum_{i=1}^n \sigma_i^z \quad (20)$$

$$+ J \frac{1+\gamma}{2} \sigma_1^y \sigma_2^z \cdots \sigma_{n-1}^z \sigma_n^y + J \frac{1-\gamma}{2} \sigma_1^x \sigma_2^z \cdots \sigma_{n-1}^z \sigma_n^x. \quad (21)$$

146 The first two terms correspond to the $1-D$ XY Hamiltonian, whereas the last two terms belong to
 147 the boundary conditions. These boundary terms can be substituted with the conventional periodic
 148 terms $\sigma_n^x \sigma_1^x$ and $\sigma_n^y \sigma_1^y$ for states with an even number of spins pointing up, and the same terms
 149 with a negative sign for states with an odd number of spins pointing up. It is worth keeping in
 150 mind that even the Hamiltonian we are working on is not strictly the same as the XY model, in the
 151 thermodynamic limit the boundary conditions do not play any role and we recover the same results.

152 Now we will demonstrate that when the Jordan Wigner transformation is applied to this term,
 153 the PBC is recovered for the fermionic operators. First, we need to write the $\sigma_1^y \sigma_2^z \cdots \sigma_{n-1}^z \sigma_n^y$ and
 154 $\sigma_1^x \sigma_2^z \cdots \sigma_{n-1}^z \sigma_n^x$ using the σ^+ and σ^- operators

$$\begin{aligned} \sigma_1^y \sigma_2^z \cdots \sigma_{n-1}^z \sigma_n^y &= -\sigma_1^+ \sigma_2^z \cdots \sigma_{n-1}^z \sigma_n^+ + \sigma_1^+ \sigma_2^z \cdots \sigma_{n-1}^z \sigma_n^- + \\ &\quad + \sigma_1^- \sigma_2^z \cdots \sigma_{n-1}^z \sigma_n^+ - \sigma_1^- \sigma_2^z \cdots \sigma_{n-1}^z \sigma_n^-, \\ \sigma_1^x \sigma_2^z \cdots \sigma_{n-1}^z \sigma_n^x &= \sigma_1^+ \sigma_2^z \cdots \sigma_{n-1}^z \sigma_n^+ + \sigma_1^+ \sigma_2^z \cdots \sigma_{n-1}^z \sigma_n^- + \\ &\quad + \sigma_1^- \sigma_2^z \cdots \sigma_{n-1}^z \sigma_n^+ + \sigma_1^- \sigma_2^z \cdots \sigma_{n-1}^z \sigma_n^-. \end{aligned} \quad (22)$$

155 Next, the Jordan-Wigner transformation is applied to the different terms that appear in the above
 156 expression using the properties shown in Eq.(4), $\sigma^z \sigma^z = 1$ and we will restrict our system to have
 157 an even number of qubits (n). First let's compute the term $\sigma_1^+ \sigma_2^z \cdots \sigma_{n-1}^z \sigma_n^+$,

$$\sigma_1^+ \sigma_2^z \cdots \sigma_{n-1}^z \sigma_n^+ = c_1^\dagger \sigma_2^z \cdots \sigma_{n-1}^z \left(\prod_{l=1}^{n-1} -\sigma_l^z \right) c_n^\dagger = c_1^\dagger c_n^\dagger. \quad (23)$$

158
 159 The rest of the terms can be computed following the same steps, the results are summarized in
 160 the following expressions

$$\begin{aligned} \sigma_1^+ \sigma_2^z \cdots \sigma_{n-1}^z \sigma_n^+ &= c_1^\dagger c_n^\dagger, & \sigma_1^+ \sigma_2^z \cdots \sigma_{n-1}^z \sigma_n^- &= c_1^\dagger c_n, \\ \sigma_1^- \sigma_2^z \cdots \sigma_{n-1}^z \sigma_n^+ &= c_n^\dagger c_1, & \sigma_1^- \sigma_2^z \cdots \sigma_{n-1}^z \sigma_n^- &= c_n c_1, \end{aligned} \quad (24)$$

161 Subsequently, the boundary term reads

$$\begin{aligned}\mathcal{H}_{BC} &= \frac{1+\gamma}{2}\sigma_1^y\sigma_2^z\cdots\sigma_{n-1}^z\sigma_n^y + \frac{1-\gamma}{2}\sigma_1^x\sigma_2^z\cdots\sigma_{n-1}^z\sigma_n^x = \\ &= c_1^\dagger c_n + c_n^\dagger c_1 + \gamma(c_n^\dagger c_1^\dagger + c_1 c_n) = c_{n+1}^\dagger c_n + c_n^\dagger c_{n+1} + \gamma(c_n^\dagger c_{n+1}^\dagger + c_{n+1} c_n),\end{aligned}$$

162 where now is easy to see that this Hamiltonian fulfills the PBC in the fermionic space.

163 2.2 Fermionic Fourier Transform (fFT)

164 Combining all the solutions outlined in the previous sections yields the Hamiltonian corresponding to
165 the XY model but now is quadratic in fermionic annihilation and creation operators c and c^\dagger instead
166 of quadratic in spin operator σ^+ and σ^-

$$\mathcal{H}_{JW} = J \sum_{i=1}^n (c_i^\dagger c_{i+1} + c_{i+1}^\dagger c_i + \gamma(c_i^\dagger c_{i+1}^\dagger + c_{i+1} c_i)) + \lambda \sum_{i=1}^n (2c_i^\dagger c_i - 1). \quad (25)$$

167 **Hamiltonians quadratic in fermionic annihilation and creation operators are ubiquitous in condensed**
168 **matter systems, describing systems of free fermionic particles. Diagonalizing this type of Hamiltonian**
169 **is a well-established process, achieved through the fermionic Fourier transform (fFT).**

170 In the second quantization, the Fourier transform is defined as

$$c_j = \frac{1}{\sqrt{N}} \sum_{k=-\frac{n}{2}+1}^{\frac{n}{2}} b_k e^{i\frac{2\pi k}{n}j}, \quad c_j^\dagger = \frac{1}{\sqrt{N}} \sum_{k=-\frac{n}{2}+1}^{\frac{n}{2}} b_k^\dagger e^{-i\frac{2\pi k}{n}j}, \quad (26)$$

171 where b_k^\dagger and b_k are the creation and annihilation operators of the fermionic Fourier modes.

172 The discrete k values are acquired establishing the translational invariance of the system by PBC

$$\begin{aligned}|x+n\rangle &= |x\rangle, \\ \sum_k e^{i\frac{2\pi k}{n}(x+n)} |k\rangle &= \sum_{k'} e^{i\frac{2\pi k'}{n}(x)} |k'\rangle.\end{aligned} \quad (27)$$

173 Then, we multiply at both sides by $\langle k|$, and applying $\langle k|k'\rangle = \delta_{k,k'}$

$$\begin{aligned}e^{i\frac{2\pi k}{n}(x+n)} &= e^{i\frac{2\pi k}{n}(x)} \rightarrow e^{i\frac{2\pi kn}{n}} = 1, \\ \frac{2\pi kn}{n} &= 2\pi m \rightarrow k = m,\end{aligned} \quad (28)$$

174 where m is an integer. Because the number of qubits (n) is even, as mentioned in Section 2.1, we can
175 choose our k values to be

$$k = -\frac{n}{2} + 1, -\frac{n}{2} + 2, \dots, -1, 0, 1, \dots, \frac{n}{2} - 1, \frac{n}{2}. \quad (29)$$

176 In the case where the number of qubits is odd, from Eq.(23) it can be seen that an extra "-" sign
177 appears in the final result obtaining APBC $-c_1^\dagger c_n^\dagger$. Then applying translational invariance we get
178 that the k possible values are the same as in the previous case. As surprising as it may seem, one
179 can expect this result if one thinks in terms of sinusoidal functions. If the period of the sinusoidal

180 function is L we will recover in $x = 0$ the same result as in $x = L$, hence we have PBC. Nonetheless,
 181 if our lattice ends in $x = \frac{L}{2}$ then we will have the same absolute value in $x = 0$ and $x = \frac{L}{2}$ but with a
 182 different sign. As a result, we have APBC. In the end, the n odd case for APBC must have the same
 183 k values as $2n$ with PBC.

184 Even though we will be only focusing on the even number of qubits case, the procedure followed
 185 for the odd case will be equivalent to the one we will describe for the even case. One can find more
 186 information about the general case and boundary conditions in Ref. [21].

187 Fermionic Fourier Transform in the XY model

188 Before computing the new terms of the XY Hamiltonian, let us first recall the fundamental properties
 189 of the FT

$$\frac{1}{N} \sum_k e^{i\frac{2\pi k}{n}(j-j')} = \delta_{j,j'}, \quad \frac{1}{N} \sum_j e^{i\frac{2\pi(k-q)}{n}j} = \delta_{k,q}, \quad (30)$$

190 where $\delta_{j,j'}$ and $\delta_{k,q}$ are Kronecker deltas, which are 0 when $j \neq j'$ or $k \neq q$ and 1 when are equals.

191 By applying Eq.(30) to each term appearing in Eq.(25), we obtain the FT of our Hamiltonian,

$$\sum_{j=1}^n c_j^\dagger c_{j+1} = \sum_{j=1}^n \left(\frac{1}{\sqrt{n}} \sum_{k=-\frac{n}{2}+1}^{\frac{n}{2}} b_k^\dagger e^{-i\frac{2\pi k}{n}j} \right) \left(\frac{1}{\sqrt{n}} \sum_{k'=-\frac{n}{2}+1}^{\frac{n}{2}} b_{k'} e^{i\frac{2\pi k'}{n}(j+1)} \right) = \sum_k b_k^\dagger b_k e^{i\frac{2\pi k}{n}}, \quad (31)$$

192

193

$$\sum_{j=1}^n c_{j+1} c_j = \sum_{j=1}^n \left(\frac{1}{\sqrt{n}} \sum_k b_k e^{i\frac{2\pi k}{n}(j+1)} \right) \left(\frac{1}{\sqrt{n}} \sum_{k'} b_{k'} e^{i\frac{2\pi k'}{n}j} \right) = \sum_k i \sin\left(\frac{2\pi k}{n}\right) b_k b_{-k}, \quad (32)$$

194

195

$$\sum_{j=1}^n c_j^\dagger c_{j+1}^\dagger = \sum_{j=1}^n \left(\frac{1}{\sqrt{n}} \sum_k b_k^\dagger e^{-i\frac{2\pi k}{n}j} \right) \left(\frac{1}{\sqrt{n}} \sum_{k'} b_{k'}^\dagger e^{-i\frac{2\pi k'}{n}(j+1)} \right) = \sum_k i \sin\left(\frac{2\pi k}{n}\right) b_k^\dagger b_{-k}^\dagger, \quad (33)$$

196

197

$$\sum_{j=1}^n c_{j+1}^\dagger c_j = \sum_{j=1}^n \left(\frac{1}{\sqrt{n}} \sum_k b_k^\dagger e^{-i\frac{2\pi k}{n}(j+1)} \right) \left(\frac{1}{\sqrt{n}} \sum_{k'} b_{k'} e^{i\frac{2\pi k'}{n}j} \right) = \sum_k b_k^\dagger b_k e^{-i\frac{2\pi k}{n}}, \quad (34)$$

198

199

$$\sum_{j=1}^n c_j^\dagger c_j = \sum_{j=1}^n \left(\frac{1}{\sqrt{n}} \sum_k b_k^\dagger e^{-i\frac{2\pi k}{n}(j)} \right) \left(\frac{1}{\sqrt{n}} \sum_{k'} b_{k'} e^{i\frac{2\pi k'}{n}j} \right) = \sum_k b_k^\dagger b_k. \quad (35)$$

200

201

The transformed Hamiltonian becomes

$$\mathcal{H}_{FT} = \sum_k \left[2 \left(\lambda + J \cos\left(\frac{2\pi k}{n}\right) \right) b_k^\dagger b_k + iJ\gamma \sin\left(\frac{2\pi k}{n}\right) (b_k^\dagger b_{-k}^\dagger + b_k b_{-k}) \right] - \lambda n. \quad (36)$$

202 As a result of working in momentum space, the XY-Hamiltonian does not contain mixed terms
 203 between first neighbors, however, it is not diagonal yet because it contains terms with opposite
 204 momentum k and $-k$ coupled.

205 For future calculations, it is beneficial to rewrite the Eq.(36) making use of the cosine function
 206 parity ($\cos(\alpha) = \cos(-\alpha)$), acknowledging that the summation takes over positive and negative k
 207 values and without carrying the constant term λn . Thereafter, the Hamiltonian is expressed as fol-
 208 lows

$$\begin{aligned} \mathcal{H}'_{FT} &= \sum_k \left[\left(\lambda + J \cos\left(\frac{2\pi k}{n}\right) \right) (b_k^\dagger b_k + b_{-k}^\dagger b_{-k}) + iJ\gamma \sin\left(\frac{2\pi k}{n}\right) (b_k^\dagger b_{-k}^\dagger + b_k b_{-k}) \right] = \\ &= \sum_k [\epsilon_k (b_k^\dagger b_k - b_{-k} b_{-k}^\dagger + 1) + i\Delta_k (b_k^\dagger b_{-k}^\dagger + b_k b_{-k})]. \end{aligned} \quad (37)$$

209 The last term can be rewritten in matrix-vector form, then the expression becomes

$$\sum_k (b_k^\dagger \quad b_{-k}) \begin{pmatrix} \epsilon_k & i\Delta_k \\ -i\Delta_k & -\epsilon_k \end{pmatrix} \begin{pmatrix} b_k \\ b_{-k}^\dagger \end{pmatrix} + \sum_k \epsilon_k. \quad (38)$$

210 Here, the definitions of $\epsilon_k = \lambda + J \cos\left(\frac{2\pi k}{n}\right)$ and $\Delta_k = J\gamma \sin\left(\frac{2\pi k}{n}\right)$ serve the purpose of enhancing
 211 the clarity of the upcoming mathematical development.

212 2.3 Bogoliubov Transformation

213 The last step to diagonalize the Hamiltonian completely is the Bogoliubov transformation. This trans-
 214 formation is used to diagonalize quadratic Hamiltonians, for instance, it is used in the Superconduc-
 215 tivity BSC theory or solid-state physics in Hamiltonians described by phononic interactions [22]. It
 216 can be understood as a change of basis, where the new base decouples the opposite momentum
 217 terms.

218 Specifically, the transformation will have a form such as

$$\begin{aligned} a_k &= u_k b_k + v_k b_{-k}^\dagger, & a_{-k} &= u_{-k} b_{-k} + v_{-k} b_k^\dagger, \\ a_k^\dagger &= u_k^* b_k^\dagger + v_k^* b_{-k}, & a_{-k}^\dagger &= u_{-k}^* b_{-k}^\dagger + v_{-k}^* b_k, \end{aligned} \quad (39)$$

219 where a_k^\dagger and a_k are the Bogoulibov fermionic annihilation and creation operators associated with
 220 pseudo-momentum k , while a_{-k}^\dagger and a_{-k} are the Bogoulibov fermionic annihilation and creation
 221 operators associated with pseudo-momentum $-k$.

222 Because we are working in a fermionic system, we have to impose the anticommutation relation-
 223 ship of these new operators

$$\begin{aligned} \{a_k, a_k^\dagger\} &= 1 \rightarrow |u_k|^2 + |v_k|^2 = 1, \\ \{a_k, a_{-k}\} &= 0 \rightarrow u_k v_{-k} + v_k u_{-k} = 0 \end{aligned} \quad (40)$$

224 To fulfill the second relationship, we use the condition $v_{-k} = -v_k$. This last condition along with
 225 Eq.(39) could be used to reverse the fermionic operator transformation. The old fermionic operators
 226 as a linear combination of the new fermionic operators are

$$\begin{aligned} b_k &= u_k^* a_k - v_k a_{-k}^\dagger, & b_{-k} &= u_k^* a_{-k} + v_k a_k^\dagger, \\ b_k^\dagger &= u_k a_k^\dagger - v_k^* a_{-k}, & b_{-k}^\dagger &= u_k a_{-k}^\dagger + v_k^* a_k. \end{aligned} \quad (41)$$

227 For our purposes, it is useful to arrange the last expression in the vector-matrix form

$$\begin{pmatrix} b_k \\ b_{-k}^\dagger \end{pmatrix} = \begin{pmatrix} u_k^* & -v_k \\ v_k^* & u_k \end{pmatrix} \begin{pmatrix} a_k \\ a_{-k}^\dagger \end{pmatrix}. \quad (42)$$

228 The next step consists of passing from a non-diagonal Hamiltonian \mathcal{H}_{FT} to a diagonal one by
229 applying a change of basis matrix, which transforms the b_k to a_k operators.

$$\mathcal{H}'_{Bog} = \sum_k \begin{pmatrix} a_k^\dagger & a_{-k} \end{pmatrix} \begin{pmatrix} u_k & v_k \\ -v_k^* & u_k^* \end{pmatrix} \begin{pmatrix} \epsilon_k & i\Delta_k \\ -i\Delta_k & -\epsilon_k \end{pmatrix} \begin{pmatrix} u_k^* & -v_k \\ v_k^* & u_k \end{pmatrix} \begin{pmatrix} a_k \\ a_{-k}^\dagger \end{pmatrix}. \quad (43)$$

230 The Hamiltonian matrix written in terms of a_k operators becomes

$$\begin{pmatrix} \epsilon_k (|u_k|^2 - |v_k|^2) + i\Delta_k (u_k v_k^* - u_k^* v_k) & -2\epsilon_k u_k v_k + i\Delta_k (u_k u_k + v_k v_k) \\ -2\epsilon_k u_k^* v_k^* - i\Delta_k (u_k^* u_k^* + v_k^* v_k^*) & -(\epsilon_k (|u_k|^2 - |v_k|^2) + i\Delta_k (u_k v_k^* - u_k^* v_k)) \end{pmatrix} \quad (44)$$

231 The Bogoliubov modes that diagonalize the Hamiltonian are found by vanishing the non-diagonal
232 terms. For this purpose, it is convenient to express u_k and v_k as

$$u_k = e^{\phi_1} \cos\left(\frac{\theta_k}{2}\right), \quad v_k = e^{\phi_2} \sin\left(\frac{\theta_k}{2}\right). \quad (45)$$

233 Substituting the last expression in the non-diagonal term of Eq.(44) and making it vanish, one gets
234 the expression

$$\begin{aligned} & -2\epsilon_k e^{\phi_1 + \phi_2} \cos\left(\frac{\theta_k}{2}\right) \sin\left(\frac{\theta_k}{2}\right) + i\Delta_k u_k u_k - (-i\Delta_k) v_k v_k = 0 \rightarrow \\ & -2\epsilon_k e^{\phi_1 + \phi_2} \cos\left(\frac{\theta_k}{2}\right) \sin\left(\frac{\theta_k}{2}\right) + \Delta_k e^{2\phi_1 + \frac{\pi}{2}} \cos^2\left(\frac{\theta_k}{2}\right) - \Delta_k e^{2\phi_2 - \frac{\pi}{2}} \sin^2\left(\frac{\theta_k}{2}\right) = 0. \end{aligned} \quad (46)$$

235 If one wishes to vanish the phase term in the expression, the relation $\phi_1 + \phi_2 = 2\phi_1 + \frac{\pi}{2} = 2\phi_2 - \frac{\pi}{2}$
236 must be fulfilled. Without loss of generality, the relative phase can be chosen as $\phi_1 = 0$ and $\phi_2 = \frac{\pi}{2}$.
237 Accordingly, the new fermionic operators a_k^\dagger and a_k are

$$\begin{aligned} a_k &= \cos\left(\frac{\theta_k}{2}\right) b_k + i \sin\left(\frac{\theta_k}{2}\right) b_{-k}^\dagger, & a_{-k} &= \cos\left(\frac{\theta_k}{2}\right) b_{-k} - i \sin\left(\frac{\theta_k}{2}\right) b_k^\dagger, \\ a_k^\dagger &= \cos\left(\frac{\theta_k}{2}\right) b_k^\dagger - i \sin\left(\frac{\theta_k}{2}\right) b_{-k}, & a_{-k}^\dagger &= \cos\left(\frac{\theta_k}{2}\right) b_{-k}^\dagger + i \sin\left(\frac{\theta_k}{2}\right) b_k. \end{aligned} \quad (47)$$

238 In addition, using the expressions $\sin(2\theta) = 2 \cos(\theta) \sin(\theta)$ and $\cos(2\theta) = \cos^2(\theta) - \sin^2(\theta)$, the
239 Eq.(46) becomes

$$\tan(\theta_k) = \frac{\Delta_k}{\epsilon_k}. \quad (48)$$

240 It is now possible to obtain the required expressions to compute the diagonal energy terms (E_k)

$$\begin{aligned}
 |u_k|^2 - |v_k|^2 &= \cos^2\left(\frac{\theta_k}{2}\right) - \sin^2\left(\frac{\theta_k}{2}\right) = \cos(\theta_k) = \frac{1}{\sqrt{1 + \tan^2(\theta_k)}} = \frac{\epsilon_k}{\sqrt{\epsilon_k^2 + \Delta_k^2}}, \\
 u_k v_k &= u_k^* v_k = \frac{i}{2} \sin(\theta_k) = \frac{i}{2} \tan(\theta_k) \cos(\theta_k) = \frac{i}{2} \frac{\Delta_k}{\sqrt{\epsilon_k^2 + \Delta_k^2}}, \\
 u_k v_k^* &= u_k^* v_k^* = -\frac{i}{2} \frac{\Delta_k}{\sqrt{\epsilon_k^2 + \Delta_k^2}}, \\
 E_k &= \sqrt{\epsilon_k^2 + \Delta_k^2}.
 \end{aligned} \tag{49}$$

241 Therefore, Eq.(43) has the diagonal form

$$\begin{aligned}
 \mathcal{H}'_{\text{Bog}} &= \sum_k \begin{pmatrix} a_k^\dagger & a_{-k} \end{pmatrix} \begin{pmatrix} E_k & 0 \\ 0 & -E_k \end{pmatrix} \begin{pmatrix} a_k \\ a_{-k}^\dagger \end{pmatrix} = \sum_k E_k a_k^\dagger a_k - E_k a_{-k} a_{-k}^\dagger = \\
 &= \sum_k E_k (a_k^\dagger a_k + a_{-k}^\dagger a_{-k} - 1) = \sum_{k=\frac{-n}{2}+1}^{\frac{n}{2}} 2E_k \left(a_k^\dagger a_k - \frac{1}{2} \right).
 \end{aligned} \tag{50}$$

242 Finally, the diagonal Hamiltonian has the form

$$\tilde{\mathcal{H}} = \sum_{k=\frac{-n}{2}+1}^{\frac{n}{2}} \left[2E_k \left(a_k^\dagger a_k - \frac{1}{2} \right) + \epsilon_k - \lambda \right], \tag{51}$$

243 where $E_k = \sqrt{(\lambda + J \cos(\frac{2\pi k}{n}))^2 + (J\gamma \sin(\frac{2\pi k}{n}))^2}$ are the energies related to having one fermion in
 244 the Bogoulibov mode k or $-k$. As a result, we have diagonalized the XY Hamiltonian.

245 3 Quantum circuit to diagonalize the XY model

246 In this section, we introduce a circuit \mathcal{U}_{dis} designed to convert the XY Hamiltonian \mathcal{H}_{XY} into a non-
 247 interacting form $\tilde{\mathcal{H}}_{\text{XY}}$, by

$$\tilde{\mathcal{H}}_{\text{XY}} = \mathcal{U}_{\text{dis}} \mathcal{H}_{\text{XY}} \mathcal{U}_{\text{dis}}^\dagger. \tag{52}$$

248

249 Using this transformation, we can obtain all eigenstates and any superposition of them in the
 250 spin basis, by preparing a product state in the computational basis and applying $\mathcal{U}_{\text{dis}}^\dagger$,

$$|XY \text{ eigenstate}\rangle = \mathcal{U}_{\text{dis}}^\dagger |\text{Comp. basis}\rangle. \tag{53}$$

251 Furthermore, we can reverse this process. Applying \mathcal{U}_{dis} to states in the computational basis
 252 allows us to obtain any spin state represented in the diagonal basis.

253 Unfortunately, constructing these disentangling circuits \mathcal{U}_{dis} for an arbitrary Hamiltonian is a
 254 challenging task. However, for models that present analytical solutions, we can try to map each step

255 into a quantum operation. For the case it concerns us, the XY Hamiltonian needs three operations:
 256 *i*) Jordan-Wigner transformation, *ii*) Fourier transform, *iii*) Bogoliubov transformation. In the end,
 257 the disentangling circuit will exhibit the structure

$$\mathcal{U}_{dis} = \mathcal{U}_{Bog} \mathcal{U}_{FT} \mathcal{U}_{JW}. \quad (54)$$

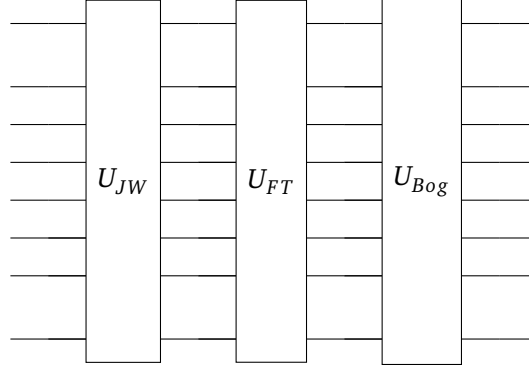


Figure 2: Schematic representation of the disentangling quantum circuit \mathcal{U}_{dis} for $n = 8$ qubits.

258 In the following section, we detail the construction of each \mathcal{U}_{dis} operation using basic quantum
 259 gates.

260 3.1 Jordan-Wigner circuit

261 The Jordan-Wigner transformation maps the spin states to a fermionic spinless mode. In terms of
 262 the wave function,

$$|\Psi\rangle = \sum_{i_1, \dots, i_n=0,1} \Psi_{i_1, \dots, i_n} |i_1, \dots, i_n\rangle = \sum_{i_1, \dots, i_n=0,1} \Psi_{i_1, \dots, i_n} (c_1^\dagger)^{i_1} \dots (c_n^\dagger)^{i_n} |0\rangle, \quad (55)$$

263 where i_j represent the state i of the qubit at position j , with j going from 1 to the number of qubits
 264 n . In spin and fermionic space, the i can take values 0 or 1. In spin space, $|0\rangle = |+\rangle$ and $|1\rangle = |-\rangle$,
 265 while in fermionic space $|0\rangle_j$ means the j -th position is not occupied by a fermion, and $|1\rangle_j$ means
 266 having one fermion.

267 Notice that the coefficients Ψ_{i_1, \dots, i_n} remain unchanged under the transformation. Thus, in the-
 268 ory, no additional gate is required to implement the Jordan-Wigner transformation. However, two
 269 important caveats must be addressed here.

270 The first one arises when two-qubit states are exchanged using a SWAP operation. Since we are
 271 dealing with fermions, exchanging two fermions requires introducing a minus sign to account for
 272 their antisymmetric nature. This adjustment is implemented using the fermionic SWAP operation
 273 (fSWAP). In matrix form, the fSWAP is represented as

$$fSWAP = \begin{pmatrix} 1 & 0 & 0 & 0 \\ 0 & 0 & 1 & 0 \\ 0 & 1 & 0 & 0 \\ 0 & 0 & 0 & -1 \end{pmatrix}, \quad (56)$$

274 which can be decomposed into a standard SWAP gate followed by a controlled-Z gate.

275 The second issue concerns a notation discrepancy. In conventional terms, spin states are denoted
 276 $|+\rangle = |0\rangle$, whereas in n -body systems the vacuum state is written as $|0\rangle$ or occasionally $|\Omega\rangle$. Since the
 277 Jordan-Wigner maps $|-\rangle$ into $|\Omega\rangle$, an X gate has been introduced to keep the standard convention
 278 and avoid potential confusion. As a result, the circuit is initialized with a layer of X gates applied to
 279 each qubit.

280 We want to stress that this decision is primarily for consistency with established conventions.
 281 Choosing not to apply X gates is a valid alternative. In such a case, the unitary transformation
 282 required to disentangle the XY model will differ slightly from the approach described in this work.
 283 However, the final result should remain unchanged.

284 3.2 Fermionic Fourier transform circuit

285 The next step involves transforming the fermionic modes into momentum space using the Fourier
 286 transform. When the number of particles is a power of two, meaning $n = 2^m$ where m is a natural
 287 number, the fermionic Fourier transform can be implemented by following the classical Fast Fourier
 288 Transform scheme [23].

289 The idea is based on the work of Andrew J. Ferrys in Ref. [24]. First, we decompose the n -qubit
 290 Fourier transform in two parallel $\frac{n}{2}$ -qubit Fourier transforms, one acting upon odd and even modes
 291 respectively

$$\begin{aligned}
 b_k^\dagger &= \frac{1}{\sqrt{n}} \sum_{j=0}^{n-1} e^{i\frac{2\pi}{n}jk} c_j^\dagger = \frac{1}{\sqrt{\frac{n}{2}2}} \sum_{j'=0}^{n/2-1} e^{i\frac{2\pi}{n}2j'k} c_{2j'}^\dagger + \frac{1}{\sqrt{\frac{n}{2}2}} \sum_{j'=0}^{n/2-1} e^{i\frac{2\pi}{n}(2j'+1)k} c_{2j'+1}^\dagger = \\
 &= \frac{1}{\sqrt{2}} \left[\frac{1}{\sqrt{\frac{n}{2}}} \sum_{j'=0}^{n/2-1} e^{i\frac{2\pi}{n/2}j'k} c_{2j'}^\dagger + e^{i\frac{2\pi}{n}k} \frac{1}{\sqrt{\frac{n}{2}}} \sum_{j'=0}^{n/2-1} e^{i\frac{2\pi}{n/2}j'k} c_{2j'+1}^\dagger \right].
 \end{aligned}
 \tag{57}$$

292 To avoid confusion with the operators defined earlier, we have chosen to use the tilde symbol
 293 to denote the operators derived from the FT in this section. In this context, b_k^\dagger is equivalent to the
 294 operator b_k^\dagger defined in Sec.2.2.

295 We can now define a new set of fermionic operators for even and odd sites $a_j \equiv c_{2j'}$ and
 296 $d_j \equiv c_{2j'+1}$. The fermionic Fourier Transform of those operators using $\frac{n}{2}$ points will be

$$\tilde{a}_k^\dagger = \frac{1}{\sqrt{\frac{n}{2}}} \sum_{j=0}^{\frac{n}{2}-1} e^{i\frac{2\pi}{n}jk} a_j^\dagger, \quad \tilde{d}_k^\dagger = \frac{1}{\sqrt{\frac{n}{2}}} \sum_{j=0}^{\frac{n}{2}-1} e^{i\frac{2\pi}{n}jk} d_j^\dagger.
 \tag{58}$$

297 If we now insert the prior definition in Eq.(57)

$$b_k^\dagger = \frac{1}{\sqrt{2}} \left[\tilde{a}_k^\dagger + e^{i\frac{2\pi}{n}k} \tilde{d}_k^\dagger \right], \quad b_{k+\frac{n}{2}}^\dagger = \frac{1}{\sqrt{2}} \left[\tilde{a}_k^\dagger - e^{i\frac{2\pi}{n}k} \tilde{d}_k^\dagger \right],
 \tag{59}$$

298 where in the last equality we have used the periodicity of the Fourier Transform. In the case of $\frac{n}{2}$
 299 Fourier Transform the period for k values is $\frac{n}{2}$, so $\tilde{a}_{k+\frac{n}{2}}^\dagger = \tilde{a}_k^\dagger$ and exactly the same for \tilde{d}_k^\dagger operator.

300 Equation (59) shows us that we can obtain the values of the n qubit Fourier Transform (b_k) from a
 301 $\frac{n}{2}$ (a_k, d_k) qubit Fourier Transform. In the case of systems with $n = 2^m$ qubits, this process of division

302 can continue iteratively until the Fourier Transform is reduced to a 2-qubit operation. Notably, the
 303 2-qubit Fourier Transform has the same expression as Eq.(59) with $k = 0$.

304 **At this stage, we have established the interplay between b_k and their counterparts a_k and d_k . Nev-**
 305 **ertheless, our primary goal is to derive the matrix that defines the relationship between $|k\rangle_b |k + \frac{n}{2}\rangle_b$**
 306 **and $|k\rangle_a |k\rangle_d$ states. This matrix can be determined by recognizing that the vacuum state remains**
 307 **unchanged under the transformation, as the Fourier Transform does not mix annihilation and cre-**
 308 **ation operators in its definition.** Hence, the remaining states can be attained by applying the creation
 309 operators to the void state, explicitly

- 310 • void vector (0 fermions) $|0\rangle_{k_b} |0\rangle_{k_b + \frac{n}{2}} = |0\rangle_{k_a} |0\rangle_{k_d}$,
- 311 • apply $b_{k + \frac{n}{2}}^\dagger$ to obtain $|0\rangle_{k_b} |1\rangle_{k_b + \frac{n}{2}} = \frac{1}{\sqrt{2}} \left[|1\rangle_{k_a} |0\rangle_{k_d} - e^{i\frac{2\pi}{n}k} |0\rangle_{k_a} |1\rangle_{k_d} \right]$,
- 312 • apply b_k^\dagger to obtain $|1\rangle_{k_b} |0\rangle_{k_b + \frac{n}{2}} = \frac{1}{\sqrt{2}} \left[|1\rangle_{k_a} |0\rangle_{k_d} + e^{i\frac{2\pi}{n}k} |0\rangle_{k_a} |1\rangle_{k_b} \right]$,
- 313 • apply $b_k^\dagger b_{k + \frac{n}{2}}^\dagger$ to obtain $|1\rangle_{k_b} |1\rangle_{k_b + \frac{n}{2}} = -e^{i\frac{2\pi}{n}k} |1\rangle_{k_a} |1\rangle_{k_d}$.

314 Here, the subscript k_b means that this vector belongs to the n -qubit Fourier space, k_a indicates that
 315 the vector is associated with the n even-qubit Fourier space, and k_d denotes that the vector belongs
 316 to the n odd-qubit Fourier space.

317 Deriving the matrix that performs the mentioned operation is a straightforward process. For the
 318 remainder of this work, we will refer to this matrix as the "General FT 2-qubit gate" or F_k^n . It takes
 319 the following form

$$F_k^n \equiv \begin{pmatrix} 1 & 0 & 0 & 0 \\ 0 & \frac{-e^{-i\frac{2\pi}{n}k}}{2} & \frac{1}{\sqrt{2}} & 0 \\ 0 & \frac{e^{-i\frac{2\pi}{n}k}}{\sqrt{2}} & \frac{1}{\sqrt{2}} & 0 \\ 0 & 0 & 0 & -e^{-i\frac{2\pi}{n}k} \end{pmatrix}, \quad (60)$$

320 where the F_k^n matrix transforms the $|k\rangle_a |k\rangle_b$ vectors into $|k\rangle_c |k + \frac{n}{2}\rangle_c$. Additionally, the 2-qubit
 321 Fourier Transform is recovered whenever $k = 0$, which is represented as F_2 .

322 It is key to bear in mind that there is a gap between the gates that can be applied theoretically in a
 323 quantum computer and those that can currently be implemented on real devices. Therefore, all gates
 324 must be decomposed into basic gates that can be implemented in a quantum computer. In certain
 325 cases, analytical schemes exist for such decompositions [25]. For the case F_k^n , the decomposition
 326 into basic gates is shown in Fig.3.

327 **Up to this point, we have found the 2-qubit gate transform. Now we will describe the circuit**
 328 **needed to perform the FT of n qubits. The approach involves decomposing the n qubits into the even**
 329 **and odd sectors, followed by applying the fermionic Fourier Transform of $\frac{n}{2}$ qubits.**

330 **Once the $\frac{n}{2}$ Fourier Transform is complete, the F_k^n gate is applied to the i qubit and the $i + \frac{n}{2}$**
 331 **qubit. This process is repeated iteratively until the FT is reduced to 2-qubit operations, which will**
 332 **be performed by F_2 . Nevertheless, depending on the connectivity of the qubits, additional fSWAP**

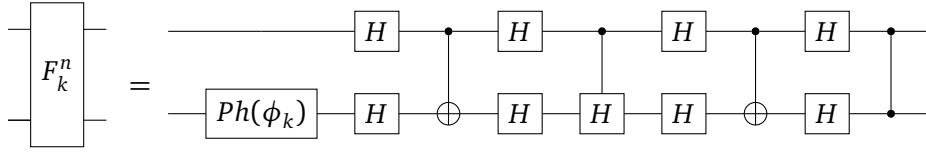


Figure 3: The diagram illustrates the decomposition of the building block of F_k^n (Eq.(60)), where $\phi_k = \frac{-i2\pi k}{n}$.

333 operations may be required. In this work, we assume a linear connectivity model, where qubits are
 334 arranged in a 1D configuration.

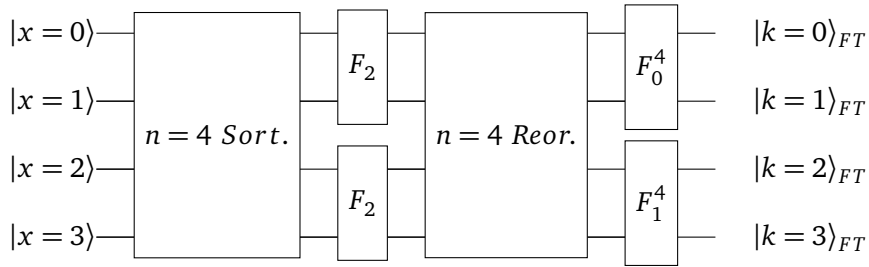


Figure 4: Scheme followed to perform the fermionic Fourier Transform (fFT) for the case of $n = 4$ qubits. The first step of the algorithm corresponds to the Qubit sorting (Sort.), then the fermionic Fourier Transform for $n = 2$ (F_2) qubits is applied and performed into the even and odd sectors. The next step is the Fourier states reorganization (Reor.) and finally, the General Fourier Transform 2-qubit gate (F_k^n) to recover the k and $k + 2$ states.

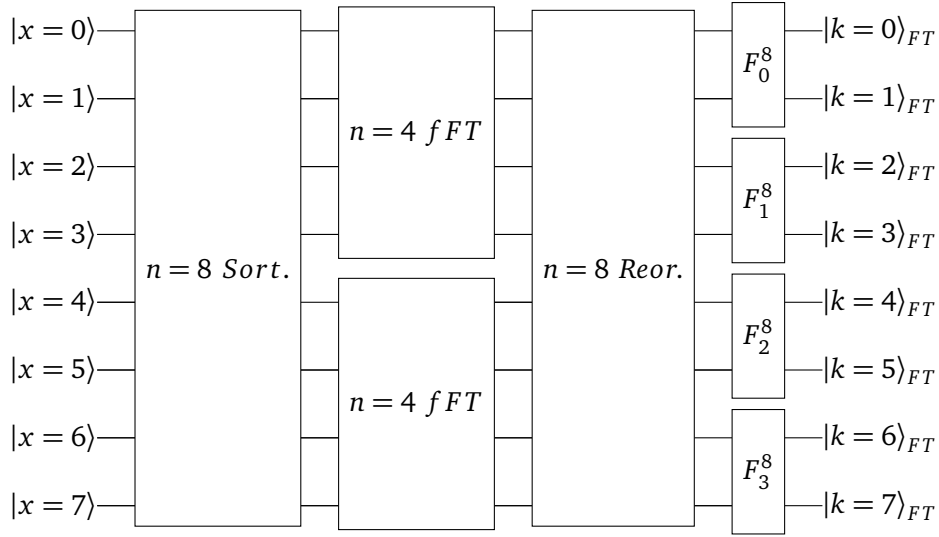


Figure 5: Scheme followed to perform the fermionic Fourier Transform (fFT) for the case of $n = 8$ qubits. The first step of the algorithm corresponds to the Qubit sorting (Sort.), then the fermionic Fourier Transform for $n = 4$ (fFT) qubits is applied and performed into the even and odd sectors. The next step is the Fourier states reorganization (Reor.) and finally the General Fourier Transform to recover the k and $k + 4$ states.

335 Next, we will describe the algorithm used to construct the fermionic Fourier Transform circuit
 336 for n qubits assuming linear connectivity and that the first qubit is numbered as 0. This circuit is
 337 decomposed into four phases:

- 338 1. **Qubit Sorting (Sort.):** In the initial step, we categorize the qubits into even and odd sectors
 339 using fermionic SWAP gates whenever we exchange two qubits.
- 340 2. $\frac{n}{2}$ **Fermionic Fourier Transform (fFT):** The second phase entails the application of the Fermionic
 341 Fourier Transform circuit for $\frac{n}{2}$ qubits into the even and odd sectors.
- 342 3. **Fourier states Reorganization (Reor.):** Subsequently, we undertake the reordering of the
 343 resulting states to group the k_{even} and k_{odd} states.
- 344 4. **General Fourier Transform Gate Application (F_k^n):** The final phase involves the application
 345 of the general Fourier transform gate F_k^n to the k_{even} and k_{odd} states. This step is performed to
 346 recover the k and $k + \frac{n}{2}$ states.

347 Figure 4 and Fig.5 represent the diagram of the fermionic Fourier Transform for the case of $n = 4$ and
 348 $n = 8$ qubits respectively. Both pictures show the different parts of the algorithm described above.

349 Qubit Sorting

350 The initial step involves the segregation of qubits into even and odd sectors through a series of
 351 fermionic SWAP operations, a process that occurs throughout $\frac{n}{2} - 1$ layers. In the first layer, precisely

352 $\frac{n}{2} - 1$ fermionic gates come into play, each consecutively applied, starting with qubit 1. Subsequently,
 353 in each successive layer, one fewer gate is used than in the previous layer, following a sequential
 354 progression starting with the next qubit after the initial qubit of the preceding layer. Moreover, in
 355 Algorithm 1, we presented the algorithm in pseudocode:

Algorithm 1 Qubit Sorting circuit

Require: $num_qubit = 2^m$

Ensure: $qc_sorting \rightarrow$ Quantum circuit which separates the qubits in even and odd sectors.

$num_label = \frac{n}{2} - 1$

$num_gates = \frac{n}{2} - 1$

$qubit_init = 1$

for $i = 1$ to num_label **do**

$count_qubit = qubit_init$

for $j = num_gates$ to 1 **do**

 add fSWAP into $count_qubit$ and $count_qubit + 1$

$count_qubit = count_qubit + 2$

end for

$qubit_init = qubit_init + 1$

$num_gates = num_gates - 1$

end for

356 To enhance the accessibility and comprehensibility of the algorithm lecture, we have illustrated
 357 the circuit for the scenario where $n = 8$ in Fig.6. This visualization aims to make the algorithm more
 358 user-friendly and easier to use.

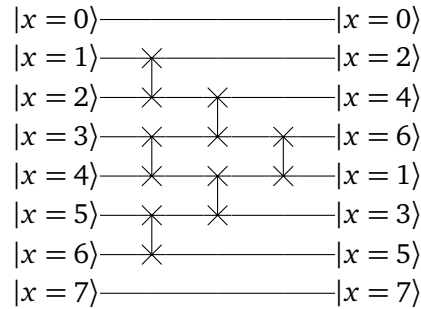


Figure 6: Qubit sorting circuit for the case of $n = 8$ qubits. Here, the fermionic SWAP gate has been represented using the same diagrammatic symbol as the SWAP gate.

359 $\frac{n}{2}$ fermionic Fourier transform

360 The next step involves applying two fermionic Fourier transforms to $\frac{n}{2}$ qubits, separately for the odd
 361 and even sectors. As a result, the transformed vector states correspond to momentum states labeled
 362 by k , ranging from $-\frac{n}{4} + 1$ to $\frac{n}{4}$ included.

363 It is important to highlight that Fourier space is periodic, specifically with a period of $\frac{n}{2}$. This
 364 periodicity allows the k states to also be labeled from 0 to $\frac{n}{2}$. In the specific case where $\frac{n}{2} = 2$,

365 the fermionic Fourier transform reduced to the application of F_0^2 , as described by Eq.(60). Figure 7
 366 illustrates the circuit scheme for the case of $n = 8$.

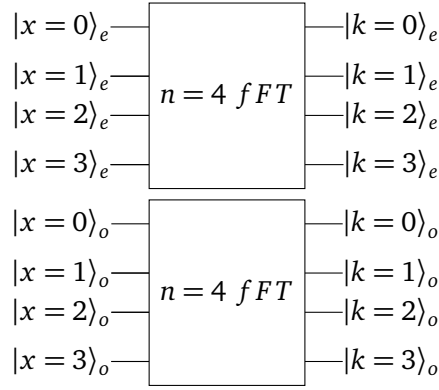


Figure 7: The $\frac{n}{2}$ fermionic Fourier transform circuit for the case of $n = 8$ qubits, the e subindex stands for even while o stands for odd. We use the periodicity of the Fourier transform, where the $k = 3$ state is equivalent to $k = -1$ state.

367 **Fourier states reorganization**

368 The reorganization phase is designed to group the newly obtained $\frac{n}{2}$ -qubit Fourier states by pairing
 369 together the k states from the even sector with the corresponding k states from the odd sector. This
 370 is achieved by the inverse circuit developed in the qubit sorting step. Figure 7 illustrates the resulting
 371 circuit for the $n = 8$ case.

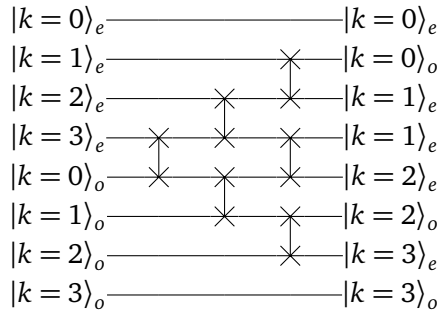


Figure 8: The Fourier states reorganization circuit for the case of $n = 8$ qubits, the e subindex stands for even while o stands for odd. Additionally, the SWAPs represented are fermionic SWAPs.

372 **General Fourier Transform Gate Application**

373 At this stage, although we have obtained k states resulting from the $\frac{n}{2}$ -qubit fermionic Fourier trans-
 374 form, we still need to recover the k states for the full n -qubit fermionic Fourier transform. To achieve
 375 this final step, the F_k^n gate must be applied to the $|k_e\rangle$ and $|k_o\rangle$ states. This operation recovers the
 376 $|k\rangle$ and $|k + \frac{n}{2}\rangle$ states associated with the n -qubit Fourier Transform.

Algorithm 2 General Fourier Transform Gate Application circuit**Require:** $num_qubit = 2^m$ **Ensure:** $qc_generalFT \rightarrow$ Quantum circuit which recovers the n Fourier transform states $|k\rangle$ and $|k + \frac{n}{2}\rangle$ from the $\frac{n}{2}$ Fourier transform states $|k_e\rangle$ and $|k_o\rangle$. $num_qubit = 0$ **for** $k_values = 0$ to $\frac{n}{2} - 1$ **do** Add the F_k^n gate to qubit num_qubit and $num_qubit + 1$ with $k = k_values$. $num_qubit = num_qubit + 2$ **end for**

377 We have illustrated the circuit for the scenario where $n = 8$ in Fig.9, to clarify the algorithm
 378 described.

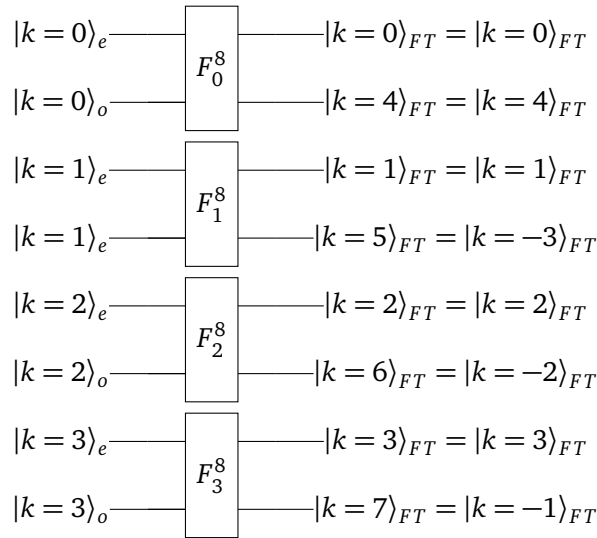


Figure 9: The General Fourier Transform Gate Application circuit for the case of $n = 8$ qubits. Furthermore, we have illustrated the equivalence between the Fourier states, denoted by the k labels ranging from $-\frac{n}{2} + 1$ to $\frac{n}{2}$ or from 0 to $n - 1$.

379 **3.3 Bogoulibov transformation gate**

380 The Bogoulibov transformation described in Eq.(47) mixes creation and annihilation operators from
 381 k and $-k$ Fourier modes. Consequently, the vacuum changes after implementing the Bogoulibov
 382 transformation. The new vacuum state $|\Omega_0\rangle$ can be found in relation to the Fourier basis $|0\rangle, |k\rangle, |-k\rangle$
 383 and $|-k, k\rangle$ imposing

384

$$a_k |\Omega_0\rangle = \left(\cos\left(\frac{\theta_k}{2}\right)\alpha - \cos\left(\frac{\theta_k}{2}\right)\gamma b_{-k}^\dagger + i \sin\left(\frac{\theta_k}{2}\right)\delta b_{-k}^\dagger + i \sin\left(\frac{\theta_k}{2}\right)\alpha b_{-k}^\dagger b_k^\dagger \right) |0\rangle = 0, \quad (61)$$

$$a_{-k} |\Omega_0\rangle = \left(\cos\left(\frac{\theta_k}{2}\right)\beta + \cos\left(\frac{\theta_k}{2}\right)\gamma b_k^\dagger - i \sin\left(\frac{\theta_k}{2}\right)\delta b_k^\dagger - i \sin\left(\frac{\theta_k}{2}\right)\beta b_k^\dagger b_{-k}^\dagger \right) |0\rangle = 0.$$

385 From the last equation, notice that $\alpha = 0$, $\beta = 0$ and $i \sin\left(\frac{\theta_k}{2}\right) \delta - \cos\left(\frac{\theta_k}{2}\right) \gamma = 0$. Using these
386 constraints, the ground state is determined as

$$\begin{aligned}
 |\Omega_0\rangle &= \delta |0\rangle + \alpha |1_k\rangle + \beta |1_{-k}\rangle + \gamma |1_{-k}1_k\rangle = \gamma \left(b_{-k}^\dagger b_k^\dagger + \frac{\cos\left(\frac{\theta_k}{2}\right)}{i \sin\left(\frac{\theta_k}{2}\right)} \right) |0\rangle \\
 \langle \Omega_0 | \Omega_0 \rangle &= |\gamma|^2 \left(1 + \frac{\cos^2\left(\frac{\theta_k}{2}\right)}{\sin^2\left(\frac{\theta_k}{2}\right)} \right) \\
 |\gamma| &= \sqrt{\frac{1}{1 + \frac{\cos^2\left(\frac{\theta_k}{2}\right)}{\sin^2\left(\frac{\theta_k}{2}\right)}}} = \sqrt{\sin^2\left(\frac{\theta_k}{2}\right)} = \left| \sin^2\left(\frac{\theta_k}{2}\right) \right|.
 \end{aligned} \tag{62}$$

387 Here, we have the freedom to choose the global phase of γ , we choose $\gamma = i \sin\left(\frac{\theta_k}{2}\right)$. Then the
388 ground state is

$$|\Omega_0\rangle = i \sin\left(\frac{\theta_k}{2}\right) |1_{-k}1_k\rangle + \cos\left(\frac{\theta_k}{2}\right) |0\rangle. \tag{63}$$

389 Note that the new vacuum vector only depends on the vacuum of the FT and the $|1_k1_{-k}\rangle$ Once the
390 new vacuum is acquired, the remaining vectors can be derived by applying the creation operators a_k^\dagger
391 and a_{-k}^\dagger

392

$$\begin{aligned}
 a_k^\dagger |\Omega_0\rangle &= \left(\cos^2\left(\frac{\theta_k}{2}\right) b_k^\dagger |0\rangle + 0 \right) + \left(0 + \sin^2\left(\frac{\theta_k}{2}\right) b_k^\dagger |0\rangle \right) = |1_k\rangle, \\
 a_{-k}^\dagger |\Omega_0\rangle &= \left(\cos^2\left(\frac{\theta_k}{2}\right) b_{-k}^\dagger |0\rangle + 0 \right) + \left(0 - \sin^2\left(\frac{\theta_k}{2}\right) b_k b_{-k}^\dagger b_k^\dagger |0\rangle \right) = |1_{-k}\rangle, \\
 a_{-k}^\dagger a_k^\dagger |\Omega_0\rangle &= \cos\left(\frac{\theta_k}{2}\right) |1_{-k}1_k\rangle + i \sin\left(\frac{\theta_k}{2}\right) |0\rangle.
 \end{aligned} \tag{64}$$

393

394 Consider that the calculations have been done assuming the order $|{-k}, k\rangle$. However, for our
395 purposes, it is more advantageous to rephrase this sequence as $|k, -k\rangle$, which entails incorporating
396 a -1 whenever the state $|11\rangle$ is interchanged. The ultimate expressions are

$$\begin{aligned}
 |0_k 0_{-k}\rangle_{Bog} &= \cos\left(\frac{\theta_k}{2}\right) |0_k 0_{-k}\rangle_{FT} - i \sin\left(\frac{\theta_k}{2}\right) |1_k 1_{-k}\rangle_{FT}, \\
 |1_k 0_{-k}\rangle_{Bog} &= |1_k 0_{-k}\rangle_{FT}, \\
 |0_k 1_{-k}\rangle_{Bog} &= |0_k 1_{-k}\rangle_{FT}, \\
 |1_k 1_{-k}\rangle_{Bog} &= -i \sin\left(\frac{\theta_k}{2}\right) |0_k 0_{-k}\rangle_{FT} + \cos\left(\frac{\theta_k}{2}\right) |1_k 1_{-k}\rangle_{FT},
 \end{aligned} \tag{65}$$

397 where we have used a different notation. The $|k, -k\rangle_{Bog}$ corresponds to the Bogoulibov states, and
398 the $|k, -k\rangle_{FT}$ corresponds to the Fourier states.

399 Once we have the Bogoulibov states written in terms of Fourier states, deriving the matrix that
400 performs this operation is straightforward. Through the remainder of this work, we will refer to this

401 matrix as the "Bogoulibov 2-qubit gate" or B_k^n . It takes the following form

$$B_k^n = \begin{pmatrix} \cos\left(\frac{\theta_k}{2}\right) & 0 & 0 & i \sin\left(\frac{\theta_k}{2}\right) \\ 0 & 1 & 0 & 0 \\ 0 & 0 & 1 & 0 \\ i \sin\left(\frac{\theta_k}{2}\right) & 0 & 0 & \cos\left(\frac{\theta_k}{2}\right) \end{pmatrix}, \quad (66)$$

402 where the B_k^n matrix transforms the $|k, -k\rangle_{FT}$ vectors into $|k, -k\rangle_{Bog}$ and θ_k is described in Eq.(48).
The basic gate decomposition of B_k^n is shown in Fig.10.

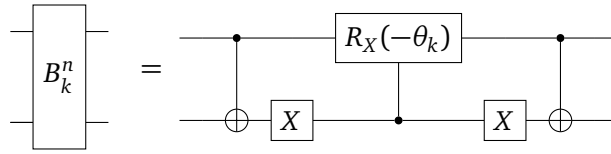


Figure 10: Decomposition of the building block of B_k^n shown in Eq.(66), where θ_k is defined in Eq.(48).

403
404

The circuit is designed to decouple the k and $-k$ Fourier modes using the 2-qubit Bogoliubov gate, denoted as B_k^n . Although this task might initially seem straightforward, its complexity increases considerably when linear connectivity is taken into account.

405
406
407
408
409
410

This added complexity stems from the requirement of additional fermionic SWAP operations to rearrange the output states produced by the fermionic Fourier Transform. Initially, these states are grouped as k and $k + \frac{n}{2}$. However, for the Bogoliubov gates to work, the states must be reorganized into pairs of k and $-k$ states.

411
412
413

Next, we will describe the algorithm used to build the Bogoulibov transformation circuit assuming linear connectivity and that the first qubit is numbered 0. This circuit is decomposed into two subcircuits:

414
415
416
417

1. **Bogoulibov Qubit Sorting:** The circuit consists of a series of fermionic SWAPS gates with the aim of grouping k and $-k$ states.
2. **Bogoulibov Gate Application:** The circuit performs the Bogoulibov transformation applying the Bogoulibov gate into the modes k and $-k$.

418 Bogoulibov Qubit Sorting:

419
420
421

The initial step involves segregating qubits into k and $-k$ modes. This can be optimally achieved by employing $\frac{n}{4} - 1$ cascades of fermionic SWAP gates, arranged according to a specific geometric pattern.

422
423
424
425
426
427

The first cascade begins at qubit 3, followed by the next cascade, which starts at the succeeding qubit after the first four gates of the previous cascade have been applied. This sequencing is crucial for optimizing the circuit's depth. If the second cascade is initiated before the completion of the fourth gate in the previous one, it would result in an incorrect sorting of states. While there are other, more straightforward geometries that can be programmed, such as applying cascades sequentially, they do increase the overall circuit depth.

428 Each cascade initially consists of $n-4$ consecutive fermionic SWAP gates, each starting where the
 429 previous one left off. Subsequently, an additional $n-5$ fermionic SWAP gates are applied sequentially,
 430 with each gate being applied one level above the previous one.

431 In Algorithm 3, we presented the algorithm in pseudocode:

Algorithm 3 Qubit Sorting circuit

Require: $num_qubit = 2^m$

Ensure: $qc_Bog_sorting \rightarrow$ Quantum circuit which groups the k and $-k$ Fourier states.

$num_cascade = \frac{n}{4} - 1$

$qubit_init = 3$

if $num_cascade = 2$ **then**

stop

else

for $i = num_cascade$ to 1 **do**

$count_qubit = qubit_init$

$down_cascade = i \cdot 4$

$up_cascade = (i \cdot 4) - 1$

for $j = 1$ to $down_cascade$ **do**

Add fSWAP into $count_qubit$ and $count_qubit + 1$

$count_qubit = count_qubit + 1$

end for

for $j = 1$ to $up_cascade$ **do**

Add fSWAP into $count_qubit - 1$ and $count_qubit$

$count_qubit = count_qubit - 1$

end for

$qubit_init = qubit_init + 1$

Start after the 4th fSWAP of the previous cascade

end for

end if

432 To enhance the accessibility and comprehensibility of the algorithm lecture, we have illustrated
 433 the circuit for the scenario where $n = 8$ in Fig.11. This visualization aims to make the algorithm
 434 more user-friendly and easier to use.

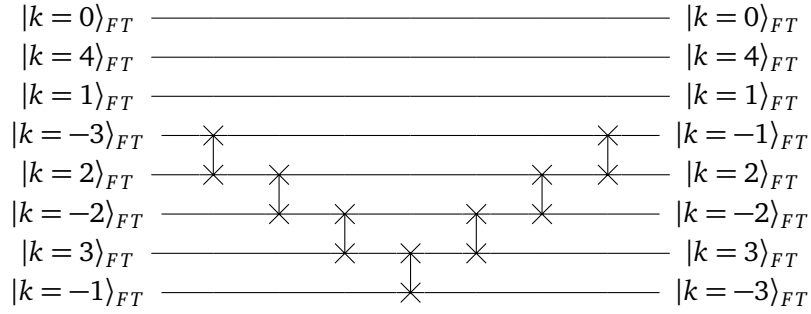


Figure 11: Bogoulibov qubit sorting circuit for the case of $n = 8$ qubits. Here, the fermionic SWAP gate has been represented using the same diagrammatic symbol as the SWAP gate.

435 Bogoulibov Gate Application:

436 Finally, we have arrived at the last step to obtain our diagonalizing circuit. To disentangle the k
 437 and $-k$ states, the Bogoulibov gate B_k^n is applied. Hence, the new circuit will be simply a layer of
 438 Bogoulibov gates, where each gate will act on the corresponding k and $-k$ states, starting from $k = 0$
 439 to $k = \frac{n}{2} - 1$.

Algorithm 4 Bogoulibov Gate Application circuit

Require: $num_qubit = 2^m$

Ensure: $qc_generalBog \rightarrow$ Quantum circuit which disentangles the $|k\rangle$ and $|-k\rangle$.

$num_qubit = 0$

for $k_values = 0$ to $\frac{n}{2} - 1$ **do**

 Add the B_k^n gate to qubit num_qubit and $num_qubit + 1$ with $k = k_values$.

$num_qubit = num_qubit + 2$

end for

440 We have illustrated the circuit for the scenario where $n = 8$ in Fig.12, where can be stated the
 441 similarity with the General Fourier Transform circuit.

442 3.4 Example: $n = 4$ and $n = 8$ spin chain

443 The explicit circuit U_{dis} for spin chains with $n = 4$ and $n = 8$ is illustrated in Fig.13, Fig.14, and
 444 Fig.15. As an example of the many applications facilitated by U_{dis} , we performed simulations to
 445 evaluate the ground state and first excited state energies of the symmetric XY model ($J = 1$ and
 446 $\gamma = 0$) for spin chains of $n = 4$ and $n = 8$, considering various values of λ . Computing the energy
 447 of the ground and first excited state enables us to observe the quantum phase transition from an
 448 antiferromagnetic to a paramagnetic state, as mentioned in Sec.2. In the symmetric XY model, the
 449 diagonalized Hamiltonian becomes

$$\mathcal{H} = \sum_{k=-\frac{n}{2}+1}^{\frac{n}{2}} 2 \left(\lambda + J \cos \left(\frac{2\pi k}{n} \right) \right) b_k^\dagger b_k - \lambda n, \quad (67)$$

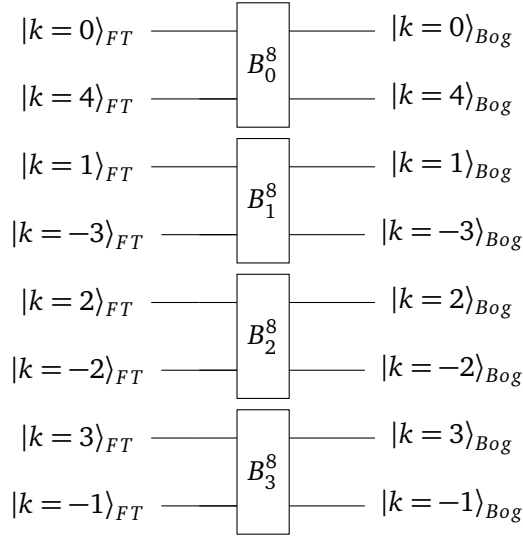


Figure 12: In the diagram is shown the Bogoulibov Gate Application circuit for the case of $n = 8$ qubits.

450 where $b_k^\dagger b_k$ is the number occupation of the Fourier states k . Notice from Eq.(48), that in the case
 451 $\gamma = 0$ the Fourier and Bogoulibov modes are equivalent. For the case $n = 4$, the ground and the
 452 first excited state written in the diagonal basis are

$$|gs\rangle = \begin{cases} |0, 1, 0, 0\rangle, & \lambda \leq 1, \\ |0, 0, 0, 0\rangle, & \lambda \geq 1, \end{cases} \quad |e\rangle = \begin{cases} |0, 0, 0, 0\rangle, & \lambda \leq 1, \\ |0, 1, 0, 0\rangle, & \lambda \geq 1. \end{cases} \quad (68)$$

453 For the case $n = 8$, the ground and the first excited state are

$$|gs\rangle = \begin{cases} |0, 1, 0, 0, 0, 0, 0, 0\rangle, & \lambda \leq 1, \\ |0, 0, 0, 0, 0, 0, 0, 0\rangle, & \lambda > 1, \end{cases} \quad |e\rangle = \begin{cases} |0, 0, 0, 0, 0, 0, 0, 0\rangle, & \lambda \leq 1, \\ |0, 1, 0, 0, 0, 0, 0, 0\rangle, & \lambda > 1. \end{cases} \quad (69)$$

454 Additionally, we have simulated the ground state for the transverse field Ising model ($J = 1$
 455 and $\gamma = 1$) in the $n = 4$ spin chain followed by the computation of the corresponding transverse
 456 magnetization. We have chosen magnetization because is one of the physical parameters which
 457 enable us to observe the phase transition discussed before. Analytically, the $\langle M_z \rangle = \sum_{i=1}^n \sigma_i^z$ in the
 458 ground state is

$$\langle gs | M_z | gs \rangle = \begin{cases} -\frac{\lambda}{2\sqrt{1+\lambda^2}}, & \lambda \leq 1, \\ -\frac{1}{2} - \frac{\lambda}{2\sqrt{1+\lambda^2}}, & \lambda \geq 1. \end{cases} \quad (70)$$

459

460 4 Time evolution

461 We have introduced the disentangling circuit U_{dis} for the 1-D XY model, which enables us to obtain
 462 the complete spectrum of the Hamiltonian. This means that we can access the full physics of the

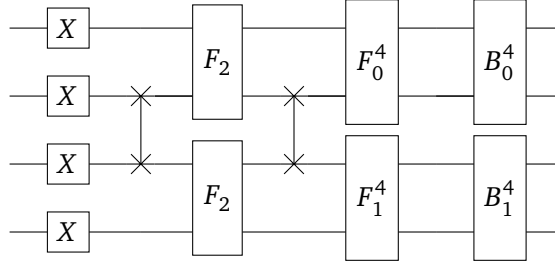


Figure 13: Quantum circuit U_{dis} designed to diagonalize the XY Hamiltonian for $n = 4$ qubits. The initial layer consists of X gates, executing the Jordan-Wigner transformation. Subsequently, F_2 and F_k^n implement the fermionic Fourier Transform. The circuit concludes with the Bogoliubov transformation achieved by B_k^n . Additionally, the swaps represented in the diagram correspond to fermionic SWAPs.

463 system by applying the disentangling circuit to the computational basis. This approach also sim-
 464 plifies the calculation of various system properties, such as the expectation values of energy and
 465 magnetization, as discussed in the preceding section.

466 However, there are instances where our focus is on computing dynamic properties. In such cases,
 467 we need to calculate the time evolution of the state, which can be a challenging task. Nonetheless, a
 468 quantum circuit can be constructed to achieve exact time evolution for fermionic Hamiltonians that
 469 can be decomposed as the sum of the energies of each particle independently,

$$\mathcal{H} = \sum_{\alpha=1}^N \epsilon_{\alpha} a_{\alpha}^{\dagger} a_{\alpha}, \quad (71)$$

470 where ϵ_{α} is the energy associated with having a particle in the state α , a_{α}^{\dagger} and a_{α} are the fermionic
 471 creation and annihilation operator of the particle in the given state.

472 The reason for constructing the time evolution gate in this case is straightforward: for such
 473 Hamiltonians, the general time evolution operator $\mathcal{U}(t)$ can be decomposed into a product state of
 474 the time evolution operator for each qubit. To illustrate this, let's express the general time evolution
 475 of a given state $|\psi(t)\rangle$ driven by a non-time-dependent Hamiltonian \mathcal{H} . The evolution is accom-
 476 plished by the unitary time-evolution operator $\mathcal{U}(t)$

$$\begin{aligned} \mathcal{U}(t) &\equiv e^{-it\mathcal{H}}, \\ |\psi(t)\rangle &= \mathcal{U}(t)|\psi_0\rangle = \sum_l e^{-itE_l} |E_l\rangle \langle E_l|\psi_0\rangle, \end{aligned} \quad (72)$$

477 where $|\psi_0\rangle$ is the initial state, $|E_l\rangle$ are the eigenstates of the given Hamiltonian, and E_l are the
 478 corresponding energies or eigenvalues of each state $|E_l\rangle$.

479 Due to the decomposable form of Hamiltonian in Eq.(71), eigenstates can be expressed as a
 480 product state of N states, each representing the presence or absence of a fermion in the α state

$$|E_l\rangle = |\alpha = 1\rangle |\alpha = 2\rangle \cdots |\alpha = N\rangle. \quad (73)$$

481 where $|\alpha\rangle$ can be represented by the qubits $|0\rangle$ or $|1\rangle$. Consequently, the time evolution operator

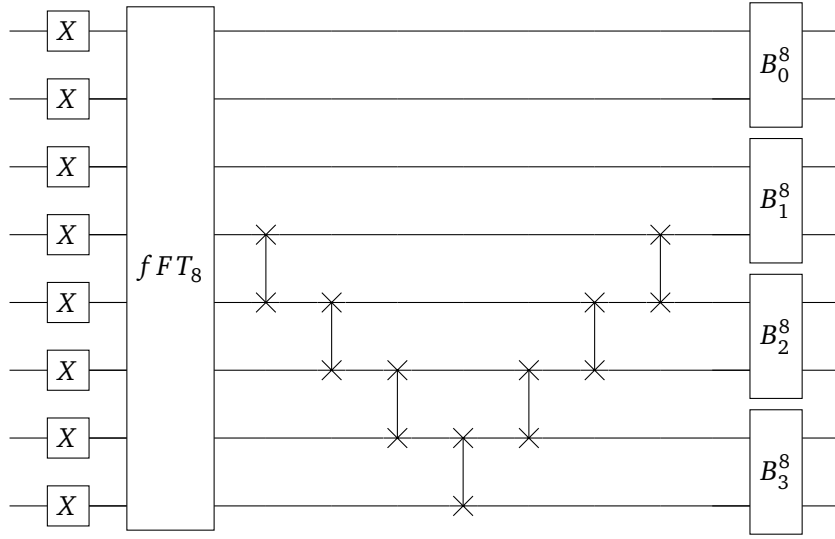


Figure 14: Quantum circuit U_{dis} designed to diagonalize the XY Hamiltonian for $n = 8$ qubits. The initial layer consists of X gates, executing the Jordan-Wigner transformation. Subsequently, the fermionic Fourier Transform is applied by the circuit fFT_8 , described in Fig.15. The circuit concludes with the Bogoliubov transformation achieved by B_k^n . Additionally, the swaps represented in the diagram correspond to fermionic SWAPs.

482 becomes

$$\begin{aligned} \mathcal{U}(t)|E_l\rangle &= e^{-it\mathcal{H}}|\alpha = 1\rangle|\alpha = 2\rangle \cdots |\alpha = N\rangle = e^{-it\sum_{\alpha=1}^N \epsilon_{\alpha} a_{\alpha}^{\dagger} a_{\alpha}}|\alpha = 1\rangle|\alpha = 2\rangle \cdots |\alpha = N\rangle = \\ &= \mathcal{U}_1|\alpha = 1\rangle\mathcal{U}_2|\alpha = 2\rangle \cdots \mathcal{U}_n|\alpha = N\rangle, \end{aligned} \quad (74)$$

483 where \mathcal{U}_i is the time evolution operator for the i_{th} qubit.

484 The procedure described above, tells us that to build the time evolution circuit we just need to
485 perform time evolution for each qubit independently. Specifically for the XY 1-D model, the time
486 evolution for the qubit representing a fermionic particle with momentum k is

$$\mathcal{U}_k = e^{-it2E_k a_k^{\dagger} a_k} e^{-it[-E_k + \epsilon_k - \lambda]} = U_1 U_2, \quad (75)$$

487 where $\epsilon_k = \lambda + J \cos(\frac{2\pi k}{n})$ and $E_k = \sqrt{(\lambda + J \cos(\frac{2\pi k}{n}))^2 + (J\gamma \sin(\frac{2\pi k}{n}))^2}$ are the energies associated
488 to having one fermion in the Bogoulibov mode k .

489 The unitary operators U_1 and U_2 can be written in matrix form

$$\begin{aligned} U_1 &= e^{-it2E_k a_k^{\dagger} a_k} = \begin{pmatrix} 1 & 0 \\ 0 & e^{-it2E_k} \end{pmatrix} = \begin{pmatrix} 1 & 0 \\ 0 & e^{i\varphi_k} \end{pmatrix}, \\ U_2 &= \begin{pmatrix} e^{-it[-E_k + \epsilon_k - \lambda]} & 0 \\ 0 & e^{-it[-E_k + \epsilon_k - \lambda]} \end{pmatrix} = \begin{pmatrix} e^{i2\Phi_k} & 0 \\ 0 & e^{i2\Phi_k} \end{pmatrix}, \end{aligned} \quad (76)$$

490 whereby $E_k = \sqrt{(\lambda + J \cos(\frac{2\pi k}{n}))^2 + (J\gamma \sin(\frac{2\pi k}{n}))^2}$ and $\epsilon_k = \lambda + J \cos(\frac{2\pi k}{n})$. Additionally, we have

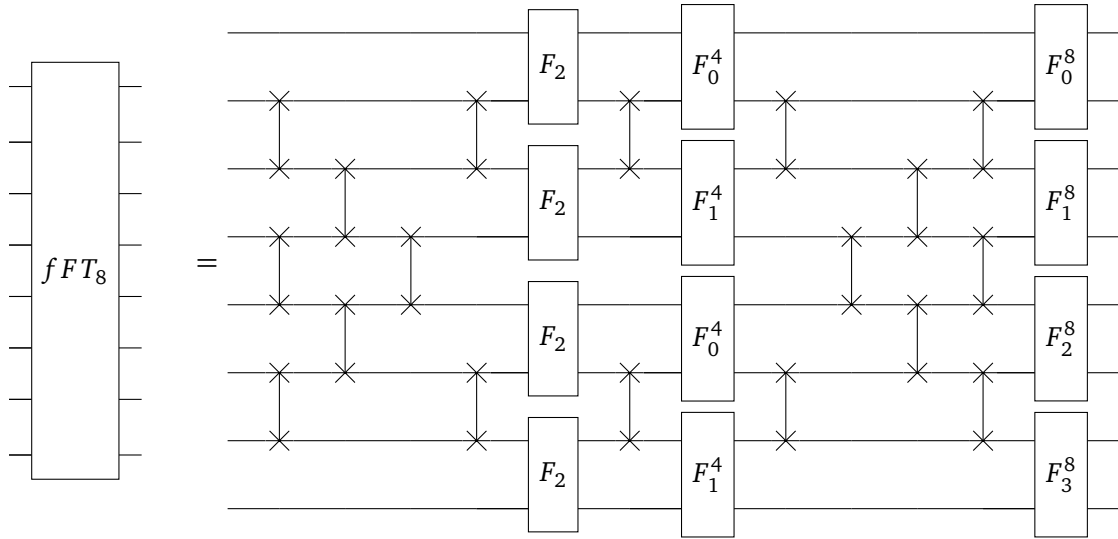


Figure 15: Fermionic Fourier Transform circuit for the case $n = 8$. The swaps represented in the diagram correspond to fermionic SWAPs.

491 renamed the exponential arguments by $\varphi_k = -2tE_k$, and $\Phi_k = -2t[-E_k + \epsilon_k - \lambda]$. The gate de-
 492 composition of \mathcal{U}_k is shown in Fig.16.

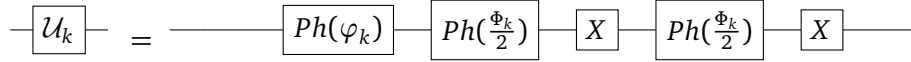


Figure 16: In the diagram is shown the decomposition of the building block of \mathcal{U}_k shown in Eq.(76), where $\varphi_k = -2tE_k$, and $\Phi_k = -2t[-E_k + \epsilon_k - \lambda]$.

493 As an example of the many possibilities this gate opens, let's compute the time evolution of
 494 the expected value of transverse magnetization for the $n = 4$ qubits case, with $J = 1$ and $\gamma = 1$.
 495 Specifically, our initial state has all the spins aligned in the positive z direction $|\psi(t = 0)\rangle = |\uparrow \uparrow \uparrow \uparrow\rangle$,
 496 which in the computational basis is written as $|0000\rangle$ state. The first step to compute the time
 497 evolution consists of expressing the initial state in the eigenbasis of the XY Hamiltonian. This is
 498 achieved by precisely applying the U_{dis} gate

$$|\psi(t = 0)\rangle = \mathcal{U}_{dis} |0 0 0 0\rangle = \sin\left(\frac{\phi}{2}\right) |1 1 0 0\rangle - i \cos\left(\frac{\phi}{2}\right) |1 1 1 1\rangle, \quad (77)$$

499 where $\phi = \arctg\left(\frac{1}{\lambda}\right)$. Subsequently, we apply the time evolution operator $U(t)$ to obtain $|\psi(t)\rangle$.
 500 Then, the time-dependent state is

$$\begin{aligned} |\psi(t)\rangle &= e^{-it2(\lambda - \sqrt{1 + \lambda^2})} \sin\left(\frac{\phi}{2}\right) |1 1 0 0\rangle - i e^{-it2(\lambda + \sqrt{1 + \lambda^2})} \cos\left(\frac{\phi}{2}\right) |1 1 1 1\rangle, \\ &= e^{-it2\lambda} e^{-i2t\sqrt{1 + \lambda^2}} \left(e^{+i4t\sqrt{1 + \lambda^2}} \sin\left(\frac{\phi}{2}\right) |1 1 0 0\rangle - i \cos\left(\frac{\phi}{2}\right) |1 1 1 1\rangle \right), \end{aligned} \quad (78)$$

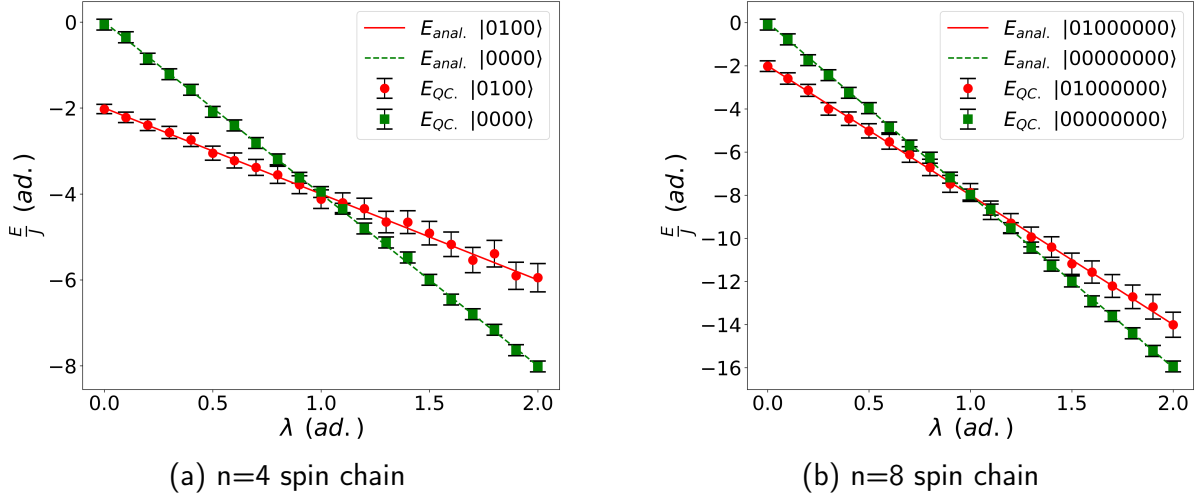


Figure 17: Study of the ground and first excited state energy for the symmetric XY model ($J = 1$ and $\gamma = 0$) as a function of the transverse field strength parameter λ . The solid (dashed) line represents the analytical values of the energy E , while the scatter points correspond to results obtained from a quantum computer simulation conducted in Qibo. (a) shows results for an $n = 4$ spin chain, and (b) for an $n = 8$ spin chain.

501 where the global phases are not physically relevant. After applying the time operator, we now apply
 502 the circuit U^\dagger to obtain the state in the spin representation. Lastly, we compute analytically the
 503 expected value of the transverse magnetization $\langle M_z \rangle$, which yields the analytical result

$$\langle M_z \rangle = \frac{1 + 2\lambda^2 + \cos(4t\sqrt{1 + \lambda^2})}{2 + 2\lambda^2}. \quad (79)$$

504 5 Results and discussion

505 In this section, we delve into the outcomes and insights derived from the application of our quantum
 506 circuit, U_{dis} , across various scenarios. **The results show the classical simulation using the quantum
 507 computing library Qibo [9], for the spin chain $n = 4$ and $n = 8$ using the circuits represented in Figs.
 508 13, 14, and 15.**

509 Figure 17 presents the outcomes of the expected energy for the ground and first excited states in
 510 the symmetric XY model ($J = 1$. and $\gamma = 0$) for spin chains with $n = 4$ and $n = 8$. Given the nature
 511 of quantum simulations, subject to inherent probabilistic uncertainties, each data point carries a sta-
 512 tistical error proportional to $\frac{1}{\sqrt{N}}$, where N represents the number of shots—indicating the executions
 513 on a quantum processing unit (QPU). Here, N was set to 1000. Notably, the results showcase the
 514 circuit's effectiveness in recovering analytical values for both cases. Moreover, a structural change in
 515 the ground state is evident at $\lambda = 1$, where the more stable state becomes the one without particles
 516 in the Bogoliubov modes k instead of having a fermion in the $-k$ mode.

517 For the transverse field Ising model ($J = 1$ and $\gamma = 1$) in the $n = 4$ spin chain, the results of the

518 ground state's expected value of transverse magnetization $\langle M_z \rangle$ are shown in Fig. 18. The circuit
 519 successfully reproduces analytical values, and at $\lambda = 1$, a magnetization discontinuity occurs due to
 520 a phase transition from an antiferromagnetic state to a paramagnetic state.

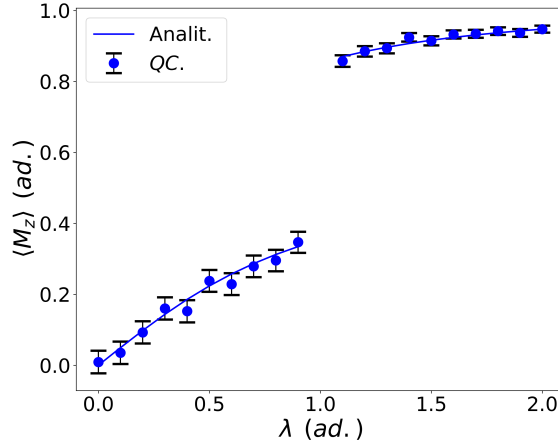


Figure 18: The ground state's expected value of transverse magnetization $\langle M_z \rangle$ for the transverse field Ising model ($J = 1$ and $\gamma = 1$) in a spin chain with $n = 4$ spins, as a function of the transverse field strength parameter λ . The solid line represents the analytical value of $\langle M_z \rangle$, while the scatter points correspond to the results obtained from a quantum computer simulation conducted in Qibo, utilizing the quantum circuit developed in this paper.

521 Moreover, we have also used the transverse field Ising model ($J = 1$ and $\gamma = 1$) to explore the
 522 time evolution of the expected value of transverse magnetization $\langle M_z(t) \rangle$. The quantum circuit $\mathcal{U}(t)$
 523 is applied to evolve the initial state $|\uparrow, \uparrow, \uparrow, \uparrow\rangle$ with the magnetic field strength fixed at $\lambda = 0.5$. After,
 524 we apply U_{dis}^\dagger to obtain the evolved spin state. The results are shown in Fig. 19, showcasing successful
 525 agreement between the quantum simulation and analytical values.

526 The circuit presented scales efficiently with the number of qubits. The Jordan-Wigner transfor-
 527 mation is a simple layer of X gate, as a result, escalates linearly with the number of qubits and the
 528 depth is constant. Similarly, the Bogoulibov transformation only combines k and $-k$ modes, result-
 529 ing in a constant circuit depth while the number of gates escalates proportionally to $\sim \frac{n}{2}$, where n
 530 represents the number of qubits. In Ref. [24], it is shown that the circuit depth of the Fourier trans-
 531 forms follows a logarithmic scaling of $\sim \log_2(n)$, with the number of gates increasing as $\sim n \log_2(n)$.
 532 The time evolution circuit scales linearly with the number of qubits n and presents a constant depth.

533 6 Conclusion

534 This paper presents a comprehensive implementation of the exact simulation of a 1-D XY spin chain
 535 using a digital quantum computer. Our approach encompasses the entire solution process for this
 536 exactly solvable model, involving key transformations such as the Jordan-Wigner transformation,
 537 fermionic Fourier transform, and Bogoliubov transformation. Additionally, we developed an algo-
 538 rithm to construct an efficient quantum circuit for powers of two qubits, capable of diagonalizing the

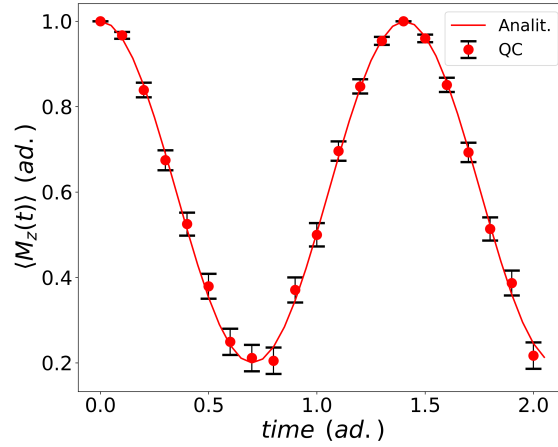


Figure 19: Time evolution simulation of transverse magnetization $\langle M_z \rangle$ for the transverse field Ising model ($J = 1$ and $\gamma = 1$) in a spin chain with $n = 4$ spins. The initial spin state is $|\uparrow, \uparrow, \uparrow, \uparrow\rangle$, evolved using the quantum circuit $\mathcal{U}(t)$ with the magnetic strength fixed at $\lambda = 0.5$. The solid line represents the analytical value of $\langle M_z \rangle$, while the scatter points correspond to the results obtained from a quantum computer simulation conducted in Qibo, utilizing the quantum circuit developed in this paper.

539 XY Hamiltonian and executing its exact time evolution. The explicit code to reproduce these circuits
 540 is presented in Ref. [15] and uses Qibo, an open-source framework for quantum computing.

541 The presented quantum circuit is a powerful tool, facilitating the calculation of all eigenstate
 542 vectors by initializing qubits on a computational basis and subsequently applying the detailed circuit.
 543 This feature enables access to the complete spectrum of the Hamiltonian, providing novel approaches
 544 for exploring various system properties, including energy, magnetization, and time evolution.

545 Our introduced quantum circuit serves as a benchmark for quantum computing devices. It
 546 presents efficient growth and scalability with the number of qubits n , making it suitable to be used in
 547 devices of diverse sizes. Furthermore, the 1-D XY model's exact solvability not only allows us to test
 548 the efficiency of real quantum computers but it offers an avenue to study and model errors inher-
 549 ent in quantum computations, establishing a bridge between theoretical predictions and real-world
 550 outcomes.

551 Beyond its utility as a benchmark, the presented quantum circuit holds intriguing applications in
 552 condensed matter physics. The methods highlighted in this work can be extended to explore other
 553 integrable models, such as the Kitaev Honeycomb model [13], or with alternative ansatz, as seen in
 554 the Heisenberg model [16].

555 Moreover, different strategies for simulating thermal evolution [11] could be employed, paving
 556 the way for new approaches to studying quantum phase transitions. Notably, the XY Hamiltonian
 557 lacks an analytical solution in two dimensions, making it particularly interesting to use the circuit
 558 to simulate the 1D case as a foundation for constructing more sophisticated methods. For instance,
 559 this could serve as a stepping stone toward approximating the ground state of the 2D system. One
 560 potential avenue to achieve this would be introducing variational interactions within the circuit to
 561 capture the effects of the 2D Hamiltonian that are absent in the 1D case.

562 In conclusion, our work contributes to the advancement of quantum computing algorithms and
563 establishes a foundation for exploring quantum solutions to complex problems in condensed matter
564 physics.

565 Acknowledgements

566 A. C.-L. acknowledges funding from the Spanish Ministry for Digital Transformation and of Civil
567 Service of the Spanish Government through the QUANTUM ENIA project call - Quantum Spain, EU
568 through the Recovery, Transformation and Resilience Plan – NextGenerationEU within the framework
569 of the Digital Spain 2026.

570 References

- 571 [1] A. K. Fedorov, N. Gisin, S. M. Beloussov, and A. I. Lvovsky, *Quantum computing at the quantum*
572 *advantage threshold: a down-to-business review*, *Quantum* **2**, 79 (2018), doi:[10.22331/q-2018-](https://doi.org/10.22331/q-2018-08-06-79)
573 [08-06-79](https://doi.org/10.22331/q-2018-08-06-79).
- 574 [2] N. S. Blunt, T. W. Rogers, J. S. Spencer, and W. M. C. Foulkes, *Density-matrix quantum Monte*
575 *Carlo method*, *Phys. Rev. B* **89**, 245124 (2014), doi:[10.1103/PhysRevB.89.245124](https://doi.org/10.1103/PhysRevB.89.245124).
- 576 [3] R. Orús, *Tensor networks for complex quantum systems*, *Nat. Rev. Phys.* **1**, 538 (2019),
577 doi:[10.1038/s42254-019-0086-7](https://doi.org/10.1038/s42254-019-0086-7).
- 578 [4] R. P. Feynman, *Simulating physics with computers*, *Int. J. Theor. Phys.* **21**, 467 (1982),
579 doi:[10.1007/BF02650179](https://doi.org/10.1007/BF02650179).
- 580 [5] J. Preskill, *Quantum Computing in the NISQ era and beyond*, *Quantum* **2**, 79 (2018),
581 doi:[10.22331/q-2018-08-06-79](https://doi.org/10.22331/q-2018-08-06-79).
- 582 [6] T. A. Chowdhury, K. Yu, M. A. Shamim, M. L. Kabir, and R. S. Sufian, *Enhancing quantum utility:*
583 *Simulating large-scale quantum spin chains on superconducting quantum computers*, *Phys. Rev.*
584 *Res.* **6**, 033107 (2024), doi:[10.1103/PhysRevResearch.6.033107](https://doi.org/10.1103/PhysRevResearch.6.033107).
- 585 [7] M. Hebenstreit, D. Alsina, J. I. Latorre, and B. Kraus, *Compressed quantum compu-*
586 *tation using a remote five-qubit quantum computer*, *Phys. Rev. A* **95**, 052339 (2017),
587 doi:[10.1103/PhysRevA.95.052339](https://doi.org/10.1103/PhysRevA.95.052339).
- 588 [8] S. I. Doronin, E. B. Fel'dman, and A. I. Zenchuk, *Simulation of three-spin evolution under XX*
589 *Hamiltonian on quantum processor of IBM-Quantum Experience*, *Quantum Inf. Process.* **20**, 264
590 (2021), doi:[10.1007/s11128-021-03181-2](https://doi.org/10.1007/s11128-021-03181-2).
- 591 [9] S. Efthymiou, S. Ramos-Calderer, C. Bravo-Prieto, A. Pérez-Salinas, D. García-Martín, A. Garcia-
592 Saez, J. I. Latorre, and S. Carrazza, *Qibo: a framework for quantum simulation with hardware*
593 *acceleration*, *Quantum Sci. Technol.* **7**, 015018 (2021), doi:[10.1088/2058-9565/ac39f5](https://doi.org/10.1088/2058-9565/ac39f5).
- 594 [10] F. Verstraete, J. I. Cirac, and J. I. Latorre, *Quantum circuits for strongly correlated quantum*
595 *systems*, *Phys. Rev. A* **79**, 032316 (2009), doi:[10.1103/physreva.79.032316](https://doi.org/10.1103/physreva.79.032316).

- 596 [11] A. Cervera-Lierta, *Exact Ising model simulation on a quantum computer*, Quantum **2**, 114 (2018),
597 doi:[10.22331/q-2018-12-21-114](https://doi.org/10.22331/q-2018-12-21-114).
- 598 [12] A. De Pasquale and P. Facchi, *XY model on the circle: Diagonalization, spectrum,*
599 *and forerunners of the quantum phase transition*, Phys. Rev. A **80**, 032102 (2009),
600 doi:[10.1103/PhysRevA.80.032102](https://doi.org/10.1103/PhysRevA.80.032102).
- 601 [13] P. Schmoll and R. Orús, *Kitaev honeycomb tensor networks: Exact unitary circuits and applica-*
602 *tions*, Phys. Rev. B **95**, 045112 (2017), doi:[10.1103/physrevb.95.045112](https://doi.org/10.1103/physrevb.95.045112).
- 603 [14] F. Shahbeigi, M. Karimi, and V. Karimipour, *Simulating of X-states and the two-qubit XYZ Heisen-*
604 *berg system on IBM quantum computer*, Phys. Scr. **97**, 025101 (2022), doi:[10.1088/1402-](https://doi.org/10.1088/1402-4896/ac49b0)
605 [4896/ac49b0](https://doi.org/10.1088/1402-4896/ac49b0).
- 606 [15] GitHub repository: <https://github.com/Marc-Farreras/XYQSimulation/tree/main>.
- 607 [16] A. J. van der Sijs, *Heisenberg models and a particular isotropic model*, Phys. Rev. B **48**, 7125
608 (1993), doi:[10.1103/physrevb.48.7125](https://doi.org/10.1103/physrevb.48.7125).
- 609 [17] A. Dutta, G. Aeppli, B. K. Chakrabarti, U. Divakaran, T. F. Rosenbaum, and D. Sen, *Quantum*
610 *phase transitions in transverse field spin models: from statistical physics to quantum information*,
611 arXiv preprint arXiv:1012.0653 (2015), doi:[10.48550/arXiv.1012.0653](https://doi.org/10.48550/arXiv.1012.0653).
- 612 [18] R. Orús, *Entanglement and majorization in (1 + 1)-dimensional quantum systems*, Phys. Rev. A
613 **71**, 052327 (2005), doi:[10.1103/PhysRevA.71.052327](https://doi.org/10.1103/PhysRevA.71.052327).
- 614 [19] P. Jordan and E. Wigner, *Über das Paulische Äquivalenzverbot*, Z. Phys. **47**, 631 (1928),
615 doi:[10.1007/BF01331938](https://doi.org/10.1007/BF01331938).
- 616 [20] M. A. Metlitski, *The XY Model in One Dimension*, Student Project for course PHYS 503, University
617 of British Columbia (2004), CorpusID: [201912290](https://arxiv.org/abs/201912290).
- 618 [21] Y. He and H. Guo, *The boundary effects of transverse field Ising model*, J. Stat. Mech. **2017**,
619 093101 (2017), doi:[10.1088/1742-5468/aa85b0](https://doi.org/10.1088/1742-5468/aa85b0).
- 620 [22] P. K. Misra, *Chapter 14 - Superconductivity*, in *Physics of Condensed Matter*, P. K. Misra, Academic
621 Press, Boston, 451–486 (2012), doi:[10.1016/B978-0-12-384954-0.00014-1](https://doi.org/10.1016/B978-0-12-384954-0.00014-1).
- 622 [23] E. O. Brigham and R. E. Morrow, *The fast Fourier transform*, IEEE Spectrum **4**, 63 (1967),
623 doi:[10.1109/MSPEC.1967.5217220](https://doi.org/10.1109/MSPEC.1967.5217220).
- 624 [24] A. J. Ferris, *Fourier Transform for Fermionic Systems and the Spectral Tensor Network*, Phys. Rev.
625 Lett. **113**, 010401 (2014), doi:[10.1103/physrevlett.113.010401](https://doi.org/10.1103/physrevlett.113.010401).
- 626 [25] A. Barenco, C. H. Bennett, R. Cleve, D. P. DiVincenzo, N. Margolus, P. Shor, T. Sleator, J. A.
627 Smolin, and H. Weinfurter, *Elementary gates for quantum computation*, Phys. Rev. A **52**, 3457
628 (1995), doi:[10.1103/PhysRevA.52.3457](https://doi.org/10.1103/PhysRevA.52.3457).